JGR Earth Surface

RESEARCH ARTICLE
10.1029/2024JF007742

Special Collection:
Prediction in coastal geomorphology

Effects of Sea Ice on Arctic Delta Evolution: A Modeling Study of the Colville River Delta, Alaska

Caroline Cooper[1], Emily Eidam[1,2], Harvey Seim[1], and Jaap Nienhuis[3]

[1]Department of Earth, Marine, and Environmental Science, University of North Carolina at Chapel Hill, Chapel Hill, NC, USA, [2]College of Earth, Ocean, and Atmospheric Sciences, Oregon State University, Corvallis, OR, USA, [3]Physical Geography, Utrecht University, Utrecht, The Netherlands

Abstract Seasonal sea ice impacts Arctic delta morphology by limiting wave and river influences and altering river-to-ocean sediment pathways. However, the long-term effects of sea ice on delta morphology remain poorly known. To address this gap, 1D morphologic and hydrodynamic simulations were set up in Delft3D to study the 1500-year development of Arctic deltas during the most energetic Arctic seasons: spring break-up/freshet, summer open-water, and autumn freeze-up. The model focused on the deltaic clinoform (i.e., the vertical cross-sectional view of a delta) and used a floating barge structure to mimic the effects of sea ice on nearshore waters. From the simulations we find that ice-affected deltas form a compound clinoform morphology, that is, a coupled subaerial and subaqueous delta separated by a subaqueous platform that resembles the shallow platform observed offshore of Arctic deltas. Nearshore sea ice affects river dynamics and promotes sediment bypassing during sea ice break-up, forming an offshore depocenter and building a subaqueous platform. A second depocenter forms closer to shore during the open-water season at the subaerial foreset that aids in outbuilding the subaerial delta and assists in developing the compound clinoform morphology. Simulations of increased wave activity and reduced sea-ice, likely futures under a warming Arctic climate, show that deltas may lose their shallow platform on centennial timescales by (a) sediment infill and/or (b) wave erosion. This study highlights the importance of sea ice on Arctic delta morphology and the potential morphologic transitions these high-latitude deltas may experience as the Arctic continues to warm.

Plain Language Summary The shape of a river delta is affected by river, wave, and tidal forces. In the Arctic, the presence of seasonal sea ice is also thought to play an important role in shaping high-latitude deltas. To investigate the effects of sea ice on Arctic delta shape, we used a popular computer model with a new representation of sea ice to examine delta growth. Our results showed that sea ice limits delta growth near the shoreline, but accelerates growth further away at sea. It leads to a large underwater platform, which is consistent with the morphology (shape) of Arctic deltas. The results were used to test future Arctic warming conditions when a reduction in sea ice coverage is likely. Future modeled simulations showed that Arctic deltas may lose the shallow underwater platform from increases in infilling by river sediments or increases in wave erosion. These results shed light on the impacts sea ice has on shaping Arctic deltas and potential changes that may occur to these delta systems as the Arctic continues to warm.

Key Points:

- 1D Delft3D simulations of delta growth under sea-ice show compound clinoform development
- Nearshore sea-ice promotes sediment bypassing and the development of a shallow subaqueous topset (2-m deep)
- Arctic deltas may lose the shallow 2-m-deep topset if future sea ice coverage continues to decline and river and wave influence grows

Supporting Information:

Supporting Information may be found in the online version of this article.

Correspondence to:

E. Eidam and J. Nienhuis,
emily.eidam@oregonstate.edu;
j.h.nienhuis@uu.nl

Citation:

Cooper, C., Eidam, E., Seim, H., & Nienhuis, J. (2024). Effects of sea ice on Arctic delta evolution: A modeling study of the Colville River Delta, Alaska. *Journal of Geophysical Research: Earth Surface*, *129*, e2024JF007742. https://doi.org/10.1029/2024JF007742

Received 19 MAR 2024
Accepted 4 AUG 2024

Author Contributions:

Conceptualization: Caroline Cooper, Emily Eidam, Harvey Seim, Jaap Nienhuis
Data curation: Caroline Cooper, Emily Eidam, Jaap Nienhuis
Formal analysis: Caroline Cooper, Emily Eidam, Harvey Seim, Jaap Nienhuis
Funding acquisition: Emily Eidam
Investigation: Caroline Cooper, Emily Eidam, Jaap Nienhuis
Methodology: Caroline Cooper, Emily Eidam, Harvey Seim, Jaap Nienhuis
Project administration: Emily Eidam

1. Introduction

Deltas are dynamic landforms; their shapes or morphologies respond to marine and fluvial conditions (Galloway, 1975; Orton & Reading, 1993). In the Arctic, this set of conditions includes ice. In its various forms such as sea ice, river ice, and permafrost, it covers Arctic landscapes for the majority of the year and plays a significant role in limiting and/or altering the morphologic effects of coastal and riverine processes on Arctic deltas (Overeem et al., 2022; Reimnitz, 2002; Walker, 1998). Sea ice, particularly landfast ice that directly contacts the delta front and/or shoreline, dissipates wave energy (Hošeková et al., 2020) and redirects fluvial sediment dispersal during key seasonal transitions (Reimnitz, 2002). However, our current knowledge of its role as a morphologic control on delta development is limited (Chan et al., 2023; Lauzon et al., 2019; Lim et al., 2019; Piliouras et al., 2021).

One of the unique distinguishing features of Arctic deltas—referred to herein as deltas located in northern Arctic plains rather than fjord systems—compared to other global deltas is their clinoforms, which are sedimentary units formed at river-marine/lacustrine boundaries (Patruno & Helland-Hansen, 2018; Pirmez et al., 1998; Swenson

Resources: Emily Eidam, Harvey Seim, Jaap Nienhuis
Software: Caroline Cooper, Emily Eidam, Jaap Nienhuis
Supervision: Emily Eidam, Harvey Seim, Jaap Nienhuis
Validation: Caroline Cooper, Jaap Nienhuis
Visualization: Caroline Cooper
Writing – original draft: Caroline Cooper
Writing – review & editing: Emily Eidam, Harvey Seim, Jaap Nienhuis

et al., 2005). Arctic deltas have a broad shallow 2-m subaqueous platform or "ramp" encircling the delta apex (Are & Reimnitz, 2000; Walker, 1998) that is similar in shape to the subaqueous "topsets" seen in many lower-latitude deltaic clinoforms (see Section 2.1). The formation mechanism for this 2-m feature in Arctic plain systems, however, is not well understood. Investigation of this feature will improve our understanding of Arctic deltaic sediment trapping and potential carbon storage (Overeem et al., 2022).

Warming Arctic temperatures are changing land-river-ocean-ice interactions on Arctic deltas by accelerating seasonal ice melt and altering the timing of sediment influx (Box et al., 2019; Overeem et al., 2022). Sea ice has experienced significant losses from rising temperatures, with a $\sim 12.7 \pm 2.0\%$ reduction in area each decade since 1979 (Meier & Stroeve, 2022). As a result, there has been an observed growth in Arctic wave energy and an increase in the amount of time that waves interact with the coastline (Barnhart et al., 2014; Casas-Prat & Wang, 2020b; Thomson et al., 2016). This shift in marine energy could significantly alter morphologic processes on Arctic deltas and thus affect biogeochemical processes (Overeem et al., 2022). Therefore, there is an emerging need to better understand the role sea ice plays in delta morphodynamics to assess the impacts of warming.

This study uses an exploratory 1D depth-averaged hydro-morphodynamic model built in Delft3D to examine cross-shore deltaic clinoform development of a simulated Arctic delta. The model applies a floating structure in Delft3D to mimic landfast sea-ice on the water surface to: (a) address how sea ice thickness, extent, and seasonality alter Arctic delta clinoform development and (b) explore potential morphologic changes related to predicted future declines in sea ice and present increases in Arctic wave energy (Barnhart et al., 2014; Casas-Prat & Wang, 2020b; Thomson et al., 2016).

Our exploratory model is loosely based on observations of the Colville River Delta, the largest delta located on the Alaskan North Slope—a region that has experienced some of the highest coastal erosion rates globally in the last decade (an average of 4.5 m/yr) due to increased wave activity (Gibbs & Richmond, 2015; Zhang et al., 2022). Model results presented here are not unique to the Colville River Delta, however, and could be used for interpretations of other Arctic delta systems with similar seasonal conditions.

2. Background

2.1. Deltaic Clinoforms

Deltaic clinoforms are sedimentary sequences that develop at some river mouths (Gilbert, 1885). Their geometry comprises three distinct features: the topset, foreset, and bottomset (Pellegrini et al., 2020; Figure 1a). The topset is a flat, low-gradient feature that extends to the rollover point, defined as the greatest inflection point seaward of the topset. Beyond the rollover point lies the foreset, which reflects the dominant zone for depositional processes and thus exhibits the highest sediment accumulation rates. The bottomset, the most distal feature, tends to have the lowest sedimentation rates due to reduced sediment supply. Similar to the topset, the bottomset begins at a defined seabed inflection point marking the foreset-to-bottomset transition. Sediment in most deltaic clinoforms tends to exhibit a coarsening-upward sequence as well as a lateral gradient in grain sizes, ranging from coarser-grained deposits proximal to the river mouth and finer-grained deposits on the distal bottomset (Patruno et al., 2015).

Studies of deltaic clinoforms have defined end-member geometries based on environmental hydrodynamics and sediment supply to describe their widely variable morphologies (Patruno et al., 2015; Pratson et al., 2007; Swenson et al., 2005; Figure 1a). End-members develop from the interplay between river and marine (e.g., wave, currents, tides, and sea-level) sediment-transport processes, which control the partitioning of sediments, and thus the overall progradation (or growth) of the delta (see Pirmez et al., 1998; Swenson et al., 2005).

For example, river-dominated deltas typically develop a single, oblique clinoform ("Gilbert-type") due to minimal marine forcing, enabling fluvial sediments to accumulate at the rollover point, creating a steep sloped surface that advances seaward over time through a slumping and rebuilding cycle (Boggs, 1995; Pratson et al., 2007; Swenson et al., 2005; Figure 1a). A well-studied river-dominated delta is the Mississippi, where high discharge dominates the basin environment (Pratson et al., 2007). In intermediate marine settings, a compound clinoform can develop (Swenson et al., 2005; J. P. Walsh & Nittrouer, 2009; Figure 1a). These consist of a coupled subaerial and subaqueous delta system, where the subaerial portion is influenced by fluvial sediment supply and the subaqueous portion is shaped and maintained by marine-driven sediment dispersal, promoting offshore deposition (Patruno et al., 2015; Swenson et al., 2005). These sedimentary structures tend to exhibit a more sigmoidal shape, with a convex upward subaqueous topset-foreset (Swenson et al., 2005; J. P. Walsh & Nittrouer, 2009), and

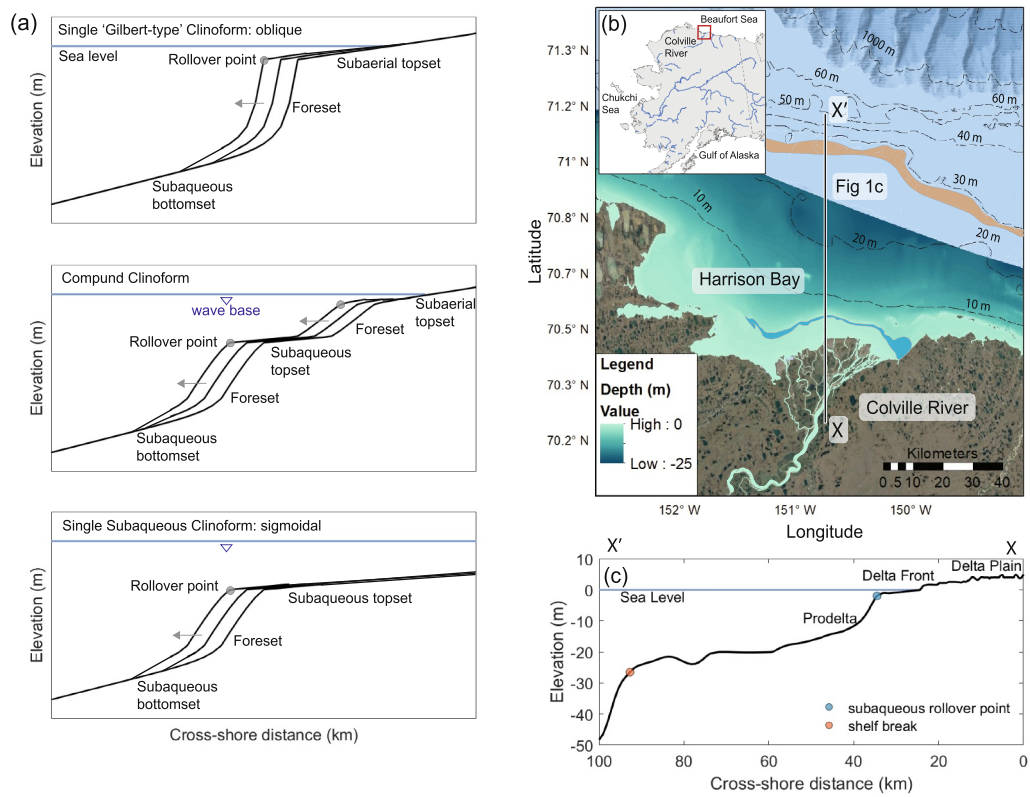

Figure 1. Overview of deltaic clinoforms compared with the Colville River Delta. (a) Conceptual diagram of three end-member deltaic clinoform geometries and defining features. (b) Location of the Colville River Delta on the Alaskan North Slope in the Beaufort Sea. Aerial imagery of the delta is from Google Earth Pro. Light teal-to-dark blue regions show digitized nearshore bathymetry data obtained from USGS overlaid on 500-m resolution bathymetry from the International Bathymetric Chart of the Arctic Ocean (IBCAO; Jakobsson et al., 2020). The blue shaded region highlights the rollover transition at the shallow 2-m subaqueous feature offshore the Colville. Orange shaded region displays the relative shelf break. (c) Cross-sectional geometry of the Colville Delta from transect line shown in plot (b). Marked points correspond to the location of the subaqueous rollover point and shelf break.

can highly vary in their vertical and lateral extent. Generally on compound clinoforms, subaerial rollover depths approximately correspond to river channel depths, whereas subaqueous rollover points can occur at depths of anywhere from 4 to 60 m, in the case of the Mekong and Ganges Delta from their differing basin dynamics (Eidam et al., 2017; Patruno et al., 2015) On the opposing end, in settings where marine basin processes are dominant and sediment supply is limited, a single subaqueous clinoform can develop (Swenson et al., 2005; J. P. Walsh & Nittrouer, 2009; Figure 1a). These subaqueous clinoforms are driven by strong marine currents that advect fluvial sediments offshore, causing the growth of these subaqueous features to outpace shoreline/subaerial delta development as in the Eel Delta (Swenson et al., 2005; J. P. Walsh & Nittrouer, 2009). Notably, these end-member descriptions are useful simplifications to classify observed features and deltaic clinoforms can vary within a given region due to changing environmental conditions (e.g., channel dynamics, wave direction).

Knowledge of the morphological influences of ice on clinoform morphology is relatively limited compared to river, wave, and tidal processes. Key work by Reimnitz (2002) provided most of the observational examples available for high-latitude deltas in the North American and Siberian Arctic, including observations of unique river and sea ice interactions and descriptions of the 2-m subaqueous feature. Modern models have focused on ice processes in the form of permafrost and ice thickness on the delta plain, and have found that permafrost and ice characteristics (thickness and extent) affect the number of active channels and can lead to offshore sediment bypassing (Chan et al., 2023; Lauzon et al., 2019; Piliouras et al., 2021). Lim et al. (2019) observed through laboratory work that nearshore ice prevented sediment deposition at the shoreline and generated sediment deposits farther offshore. Results from these previous studies suggest that ice-affected deltas would classify as a compound clinoform similar to those influenced by intermediate wave and tidal processes. However, the long-

term influence of sea ice on delta morphology remains poorly constrained, as does the role of ice as a dominant morphologic control under mixed seasonal conditions. To investigate this, we examined the interactions between sea ice and the formation of deltaic clinoforms, assessed varying seasonal conditions, and analyzed the impact of incorporating wave dynamics.

2.2. The Colville River Delta

Many of the open questions that still surround Arctic delta morphology can be viewed from the perspective of the Colville Delta, which has morphological patterns that are typical of the Arctic. The Colville Delta is the largest delta on the Alaskan North Slope with a delta plain area of ~600 km^2 (Walker, 1998; Figure 1b). Like many global deltas, its growth began ~5–6 kya when rapid Holocene sea-level rise decelerated (Overeem et al., 2022; Walker, 1998). The Colville can be classified as river-influenced, as mouthbars have formed a distributary network (Galloway, 1975; Nienhuis et al., 2020; Overeem et al., 2022). Tidal influence on the delta is minimal because the range is microtidal (10–20 cm; NOAA station 9497645, Prudhoe Bay, AK). There is also no clear seaward expansion of channel width that would be expected when tidal flows dominate in the delta channels (Figure 1b).

The Colville Delta morphology is heavily influenced by ice processes. The subaerial portion of the delta is marked by a complex distributary channel network overlaid with ice-wedge polygons and shallow thermokarst lakes, which are depressed lakes that form in thawing ice-rich permafrost (Piliouras & Rowland, 2020; Walker, 1998). Approximately 25% of the subaerial delta consists of thermokarst lakes (Piliouras & Rowland, 2020). Sediments on the delta plain consist of 2 and 3 m thick mud and peat deposits sourced from the late Pleistocene and Holocene, which overlay marine, alluvial, and glacial-fluvial sediments from the Gubik Formation deposited during the Quaternary (Reimnitz et al., 1985).

Offshore, subaqueous deposits along the 2 and 3 m isobath have been characterized as fine, well-sorted sand, which transitions to poorly sorted sandy mud toward the slope break at ~27 m water depths (Eidam, 2023; Reimnitz, 2002; Reimnitz & Bruder, 1972). Much of the subaqueous delta comprises a prominent shallow region referred to as a 2-m subaqueous ramp that extends seaward 5–10 km (~15% of the cross-shore distance to the shelf break; Figure 1c). Its formation has been attributed to nearshore landfast ice (sea ice that grounds or "fastens" to the land and grows from the coast seaward), which extends 15–20 km from the shoreline and can grow up to 2 m thick (Reimnitz & Bruder, 1972). However, there are regions along the Alaskan Beaufort coast with no river sourced sediments that also exhibit a subaqueous ramp (0.5–5 km width), which suggests that other or multiple processes may play a role in its formation (Reimnitz, 2002; Reimnitz et al., 1985). The 2-m ramp features noticeable ice gouging, likely caused by pressure ridges formed from converging sea ice (Eidam et al., 2022; Reimnitz & Bruder, 1972; Reimnitz et al., 1985). This portion of the delta also features meters-wide strudel scours, which develop when river water energetically flows through cracked sea ice, impacting the seabed (Eidam et al., 2022; Reimnitz & Bruder, 1972; Reimnitz et al., 1978).

2.3. Seasonality in the Colville Delta

Ice extent, thickness, and duration are strongly seasonal in Arctic rivers and deltas, including the Colville Delta. Ice cover typically extends from early November to late-May (Walker & Hudson, 2003). During this season, Colville River discharge effectively ceases, and offshore currents rarely exceed 5 cm/s (Weingartner et al., 2017). Ice reaches its maximum thickness of 1.5–2.5 m toward the end of the season, with some ice growing deep enough to attach to the seabed, forming bottomfast ice (Overeem et al., 2022; Reimnitz et al., 1978). Bottomfast ice has been observed to form along the shallow 2-m subaqueous platform on the Colville (Dammann et al., 2018; Reimnitz, 2002).

Around late May, as air and river temperatures rise, river ice breaks up and discharge increases. Floodwaters inundate the delta plain (Walker & Hudson, 2003), flowing over and under ice, melting nearshore landfast ice, and detaching bottomfast ice from the seabed (Reimnitz & Bruder, 1972; Walker, 1973). In the 20-year river discharge record, the average duration of river ice break-up spans approximately 3 weeks each year. Based on limited data, the river may supply ~40% of its annual water discharge during this time (Arnborg et al., 1967), and a maximum discharge of 7.0×10^3 m^3/s has been observed from a modern 20-year record (USGS gauge 15875000). Past studies have recorded maximum current speeds up to 2 m/s under the river ice and the spring freshwater plume traveling 40 km offshore under sea ice (Arnborg et al., 1966; Reimnitz & Bruder, 1972;

Walker, 1973). Data on the sediment load of the Colville River are sparse, though according to a study conducted in 1962, 75% of the annual sediment load (5.9×10^{10} kg) is released during break-up (Arnborg et al., 1967). Sediment is delivered to the connected thermokarst lakes, delta plain, and on top of and under the nearshore landfast ice during this season (Reimnitz, 2002; Walker, 1973). Sediments deposited on the top of ice account for ∼2% of the total annual sediment load, and the percent transported under ice remains poorly constrained (Reimnitz & Bruder, 1972).

After the break-up, as river and sea ice continue to melt, the Colville River begins to flow freely and the marine influence on the delta front increases, coinciding with the open-water season in the Arctic. Discharge decreases to a summertime average of ∼300 m^3/s, with occasional peaks exceeding 1,000 m^3/s due to pluvial events later in the summer and fall. Fetch increases while sea ice retreats throughout the summer, allowing increasingly large waves to form (Eidam et al., 2023; Reimnitz et al., 1985). During the beginning of the open-water season, prevailing northeasterly winds create an overall net westward transport of sediments offshore of the Colville (Reimnitz et al., 1985). As sea ice reaches its minimum extent in the Arctic Ocean around late August/early September, the Colville Delta experiences a more bimodal wind pattern of northeasterly and northwesterly winds from the increase in westerly storm events (Reimnitz et al., 1985). These storms can last for several days, producing surges exceeding 1 m that inundate the delta front and transport large volumes of terrestrial sediment seaward (Reimnitz et al., 1985).

In mid-October, river and landfast sea ice starts to develop (Mahoney et al., 2007; Walker & Hudson, 2003). River ice forms first, followed by landfast sea ice in the nearshore zone with the onset of cooler atmospheric and land temperatures (Walker & Hudson, 2003). Arctic storms persist throughout ice freeze-up. Landfast ice/storm-wave interactions have been observed to dissipate storm-wave energy during this period (Hošeková et al., 2020; Smith & Thomson, 2016). Ice completely covers the Colville Delta again by November, limiting further geomorphic activity until the following year (Walker & Hudson, 2003).

2.4. Climate Change in the Colville Delta

Seasonal cycles at the Colville are shifting with warming Arctic temperatures and the loss of sea ice. Sea ice break-up on the Beaufort Sea has begun on average ∼0.3 days earlier per year, and freeze-up has started ∼0.6 days later per year since 1979 (J. E. Walsh et al., 2022). Overall, these seasonal shifts have extended the open-water season in the Arctic Ocean by 3.9–14 days per decade from 1979 to 2016 (Bliss et al., 2019). Sea ice loss has allowed increases in wave heights and more impacts from storm events (Thomson & Rogers, 2014). Climate models predict a >0.5% per year growth in significant wave heights with a decline in minimum sea ice extent (Casas-Prat & Wang, 2020a). Additionally, the Arctic hydrological cycle is expected to intensify due to warming, leading to increases in discharge and changes in the timing of the spring freshet. Currently, there is no significant trend in annual total discharge from the Colville River according to time-series records (USGS gauge 15875000). However, spring freshet among the North Slope rivers (Colville, Kuparuk, and Sagavanirktok) has been observed to occur on average 4.5 days earlier (Rawlins et al., 2019). Models examining freshwater export from the Colville River indicate a potential 215% increase in discharge during the current ice-covered season (Rawlins et al., 2019). These increases in discharge combined with permafrost thaw are predicted to increase fluvial sediment discharge by 22% with every 2°C of atmospheric warming (Syvitski, 2002). The described changes in seasonal dynamics could affect the morphology of the Colville Delta; however, the scale and timing of this impact remain unknown.

3. Methods

3.1. Model Description

A simplified 1D depth-averaged model was constructed in Delft3D (see Lesser et al., 2004) to simulate the cross-shore effects of seasonal sea ice and waves on Arctic delta evolution. The model was coupled with modules written in MATLAB to simulate seasonal cycles of sea ice, sediment discharge, and waves representative of the Colville River Delta environment.

In assessing the role of sea ice, model simulations were divided into two timescales: long-term delta developmental runs (spanning 1500 years) and future scenario runs (spanning 450 years). Delta developmental simulations included ice-free and ice-affected cases. These cases consisted of simulations with and without waves to compare sea ice, river, and wave impacts on Arctic delta evolution. Nine varying sea ice conditions were also

Table 1
List of Model Runs

Model run names	Description	Modeled time (yr)
Ice-free	Comparative control run	1500
Ice-affected	Seasonal sea ice on delta clinoform development	1500
Ice-free with waves	Comparative control run with waves	1500
Ice-affected with waves	Seasonal sea ice and waves on delta clinoform development	1500
Ice matrix ($n = 9$)	Varying sea ice thickness and location on delta clinoform development	500
Future scenario A	Exploratory run: future Arctic delta evolution with less sea ice	450
Future scenario B	Exploratory run: future Arctic delta evolution with less sea ice and larger waves	450

evaluated to examine ice characteristics on delta development for the first 500 years. Additionally, two versions of future scenarios were assessed: (a) a longer open-water season; and (b) increased wave energy during the open-water and freeze-up seasons. A full summary of model simulations is presented in Table 1.

3.1.1. Model Setup

The initial model domain was a 150 × 1 km grid with 300-m horizontal cell size and an assigned basinward slope of 4.18×10^{-4} m/m (Figure 2; Table 2). Slope calculations were extrapolated from surface elevation measurements in Google Earth Pro using the National Elevation Data set from USGS, combined with 500-m resolution publicly available IBCAO bathymetry (Jakobsson et al., 2020) and inner-shelf digitized bathymetry obtained from USGS (Figures 1b and 1c). The elevation transect started at the apex of the delta (where distributaries begin branching) and continued to the shelf break at ~27 m depth (Figures 1b and 1c). The model was forced by two boundary conditions: (a) a water-level boundary; and (b) a total discharge (river) boundary. The water-level boundary was located at the seaward end of the domain at 65 m water depth (Figure 2). Phase-averaged waves were implemented using the Delft3D-FLOW surfbeat roller model (Deltares, 2014). The discharge (river) boundary was located upstream, with an initial depth of 2.5 m, which reflects the approximate depths of the Colville River channels (Mikhailova, 2009).

The 1D model design has some implications for the outcomes. Over long timescales, the model delta progradation will not decelerate over time as much as most radially expanding natural deltas. Over shorter timescales, our simulations will also not capture dynamics such as lobe shifts.

To simulate the effects of sea ice, a floating structure was positioned on the part of the water surface, with its size and location varying seasonally. When present, a local surface pressure was assigned to the floating structure, which compressed surface waters to the selected depths (Deltares, 2014). An artificial compression coefficient of 1.0 was applied to the floating structure parameter to restrict movement of the free surface and stabilize the flow of water and sediments under the structure (Deltares, 2014; Goede et al., 2014). Additionally, an upwind advection scheme was applied to ensure model stability.

Basin salinity and river temperature dynamics were excluded from the model parameters as they would be poorly represented in a 1D model and would cost computational time, especially for 1500-year model runs. Sediment parameters were adjusted to account for the exclusion of salinity (0 ppt) and to mimic the effects of flocculation (e.g., settling velocity). We note that by excluding these parameters, the model did not account for density-driven

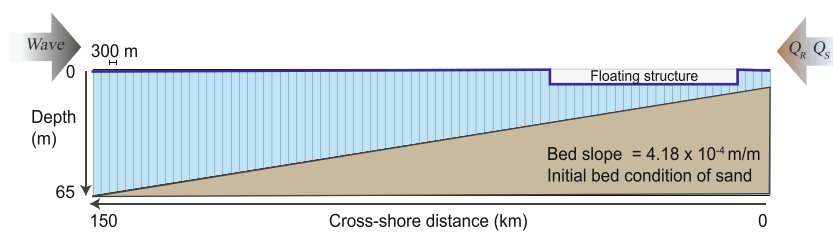

Figure 2. Schematized model domain.

Table 2
User-Defined Model Parameters

Constant between model runs	Value	Units
Grid size	150 × 1.00	km
Cell size	0.300 × 1.00	km
Initial basin bed slope	4.18×10^{-4}	m/m
Initial sediment layer thickness at bed	10.0	m
Subsurface stratigraphy bed layer thickness	0.150	m
Number of subsurface stratigraphy bed layers	50	–
Time step	0.200	min
Spin-up time interval before morphological updating begins	180	min
Sand d_{50}	110	μm
Sand dry bed density	1590	kg/m^3
Cohesive sediment dry bed density	1060	kg/m^3
Cohesive sediment settling velocity	1.00	mm/s
Cohesive sediment critical shear stress for erosion (τ_c)	0.800	N/m^2

Seasonal between model runs	Break-up	Open-water	Freeze-up	
Morphological scale factor (MF)	16.0	103	30.0	–
Sea ice thickness[a]	2.00	–	–	m
Sea ice offshore extent	20.0	–	–	km
Q_R at the total discharge boundary	4.00×10^2	2.50×10^2	1.00×10^2	m^3/s
Q_S at the total discharge boundary	1.73×10^{-2}	8.20×10^{-3}	2.70×10^{-3}	kg/m^3
Historical H_s at water level boundary	–	0.200	0.600	m
Historical T_p at water level boundary	–	5.00	5.00	s
Future scenarios MF	16.0	155	30.0	–
Future H_s at water level boundary[b]	–	0.800	2.00	m
Future T_p at water level boundary[b]	–	7.00	7.00	s

Note. Footnotes denote certain conditions used in different model simulations. [a]Sea ice thickness used in delta developmental and future scenario simulations. [b]Future wave climate was only used in the model run scenario B.

hydrodynamics that can significantly alter fluvial sediment delivery to a basin by riverine plumes or exchange flow dynamics (Kasper & Weingartner, 2014; Syvitski et al., 2019). Additionally, these parameters are known to affect sea ice melt/formation (Stroeve & Notz, 2018), which was not explored in the model since nearshore sea ice was represented by a floating structure.

Two sediment classes were applied in the model at the river boundary: sand (representative of bedload) and mud (representative of suspended load; Table 2). Sand was classified as a non-cohesive sediment and assigned a d_{50} of 109.7 μm and dry bed density of 1,590 kg/m^3. Cohesive mud was assigned a settling velocity of 1 mm/s but not a grain size, and a dry bed density of 1,060 kg/m^3. The settling velocity was assigned a value of 1 mm/s to represent flocs. Additionally, the critical shear stress for erosion of cohesive sediments was set to a relatively high value of 0.8 Pa to account for the consolidated permafrost sediments that comprise the Arctic seascapes (Brilli, 2023). Sediment characteristics used in the model were determined from grab samples and cores collected offshore in Harrison Bay during the summer 2020, 2021, and 2022 field seasons as well as from previously published literature (Brilli, 2023; Eidam, 2023; Malito et al., 2022; Walker, 1994). Sediment discharge in the model, Q_S, was derived from a rating curve (Figure 3b) extracted from Arnborg et al. (1967) study applied to discharge, Q_R, from USGS gauge at Uimat, AK.

Fluvial sediment concentrations from the river boundary consisted of 10% sand and 90% mud, based on the typical ratio between bedload and suspended load transport for global river systems (Pratson et al., 2007). This conservative ratio was based on global data due to the lack of information on the Colville River sediment

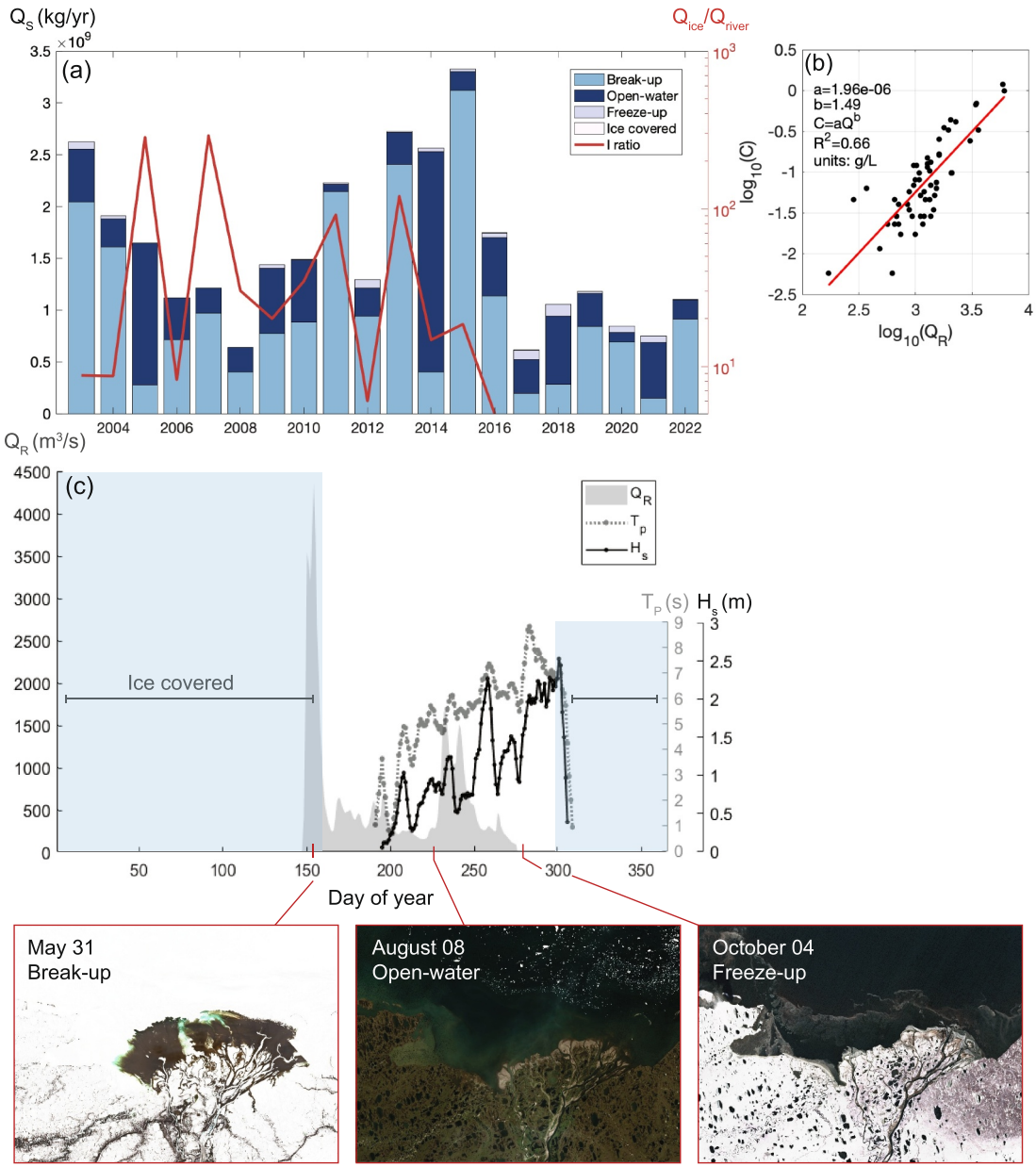

Figure 3. Seasonal sediment and hydrodynamics of the Colville River Delta. (a) Annual sediment load, Q_S, of the Colville River derived from the Arnborg et al. (1967) data and the rating curve in (b) applied to USGS discharge measurements in (c) (see text). Sediment loads are divided by seasonal inputs. Annual I ratio is shown in orange, see Section 3.3, and derived from ice-cover data from Overeem et al., 2022. (b) Colville River sediment-rating curve generated from Arnborg et al. (1967). (c) Example of annual hydrograph of Colville Delta from USGS gauge 15875000 at Umiat, AK (from 2022) and the wave climate from ERA5 reanalysis (from 2022; see text). Discharge, Q_R, is shown in shaded gray, peak wave period, T_P, is shown as a dashed gray line and significant wave height, H_S, is shown in black. Satellite imagery of the Colville Delta from 2022 showing the various modeled seasons. Imagery is Sentinel-2 data acquired from Copernicus data visualization (https://browser.dataspace.copernicus.eu).

composition. The initial seabed condition in the domain was a 10-m-thick layer of sand to act as a basement for the modeled deltaic deposits. The underlayer parameter in Delft3D was employed to track bed stratigraphy produced during delta development for different model runs.

3.1.2. Seasonality in the Model

In this study, every year each Arctic season (break-up, open-water, freeze-up) was run as a separate 24-hr model simulation. This is because the floating structure cannot vary in time or space during a continuous model

simulation; therefore, looping through restart files allowed for unique sea ice, discharge, sediment, and wave conditions to be imposed (Table 2). Each 24-hr "season" was then multiplied by a morphological scaling factor (MF) in order to represent morphological change according to the differing length of each season (Table 2). Bathymetry continuously evolved from one season to the next, but hydrodynamics were re-initiated every time. A spin-up interval of 180 min was applied at the start of each season to allow hydrodynamics to stabilize before any morphologic change occurred. Individual season model runs were assigned a timestep of 0.2 min. The long winter ice-covered season was not modeled because river discharge and sediment transport are minimal (Figures 3a and 3c), and excluding this season saved computation time.

Various model sensitivity tests were conducted to ensure that changing seasonal parameters did not affect the outputs. For example, we examined seabed differences between simulations with no MF and with MF, finding less than ±0.1 m difference in deposition, and determined that the results were independent of the applied MF.

3.2. Model Scenarios

3.2.1. Long-Term Delta Development

To simulate long-term Arctic delta development in the model, simulations were conducted over 1500 years, with each year characterized by different sea ice and sediment discharge conditions. Within a given year, the break-up season was defined in the model as a 14-day period and was assigned 75% of the annual sediment load. The open-water season was defined as a 90-day period and accounted for 22% of the annual sediment load, followed by the freeze-up season (30 days, 3% of annual sediment load).

Floating sea ice was imposed only during the break-up season to recreate typical natural conditions (Figure 3c). Sea ice extended for 20 km seaward with a thickness (depth) of 2 m and was initially established with a separation of 1 km offshore of the river mouth (Table 2). During the simulation, sea ice remained in its initial position until shoreline development; then, the ice moved seaward synchronously with delta progradation.

3.2.2. Varying Sea Ice Characteristics

Nine 500-year simulations ("ice-matrix") were run to assess the impact of varying sea-ice characteristics (extent and thickness) on delta clinoform development. Ice thicknesses of 0.5, 1, and 2 m, and locations of 0.5, 1, and 2 km relative to the river boundary, were chosen based on observational studies of seasonal sea ice coverage along the Alaskan North Slope (Mahoney et al., 2007; Reimnitz & Bruder, 1972; Weingartner et al., 2017). The shoreline offset distance and ice thickness were varied in order to study delta sensitivity to ice characteristics, such as a larger open-water space during spring breakup (represented by the shoreline offset) and thinner ice (which might be expected given warmer water temperatures). In these model cases, river boundary and MF inputs were the same as those shown in the original long-term runs (Table 2), but simulations did not include waves.

3.2.3. Future Scenarios

Two future Arctic sea-state scenarios were evaluated based on present warming conditions: Future scenario A, which included a 50% increase in the modeled open-water season (which represents a conservative projection from the study by Barnhart et al. (2016), who showed similar increase in a shorter time span); and future scenario B, which included a 50% increase in the modeled open-water season and an increase in wave energy during the open-water and freeze-up seasons (also, a conservative projectation from ERA5). These model simulations were run for 450 years using the restart file from the 1100-year timestamp of the long-term delta developmental run (ice-affected with waves; Table 1). This restart file was used in lieu of the 1500-year restart file due to a time limitation within the model configuration. This was not considered problematic because the overall bathymetric changes (e.g., length and depth of clinoform features) in the chosen restart timestamp had reached steady progradation rates.

In future scenario A, a 50% increase in open-water days was applied and the MF was increased from 103 to 155, which increased the modeled open-water season duration from 90 to 135 days (Table 2). In turn, this change increased the annual time of fluvial forcing from 130 to 175 days, and the exposure to waves from ∼50 to ∼70 days. To maintain a consistent sediment load with the increased MF compared to long-term simulations, the Q_R and Q_S during the open-water season were lowered to 200 m^3/s and 6.79×10^{-3} kg/m^3, respectively. This

reduced sediment supply was implemented in order to facilitate an equal comparison between the reference (long-term ice affected) and future simulations.

In future scenario B, larger wave heights and longer wave periods were imposed on the longer open-water season and larger MF imposed in future scenario B. This study was designed to simulate the morphologic effects of an increased wave climate together with diminished sea ice. The assigned wave climate during these periods represents the relative averages reported by the recent ERA5 wave hindcast (Figure S1 in Supporting Information S1).

3.3. Model Analysis

Model simulation outcomes were assessed in terms of hydrodynamics, sediment transport, morphodynamics, and the resulting stratigraphy. The morphology of each outcome is quantified by the location of the shoreline, rollover point(s), and inflection point(s); the gradient, length, and height of the topset, foreset, and bottomset; accumulation rates; and sediment stratigraphy. The shoreline position was defined as 0 m in elevation. Inflection and rollover points were identified as the absolute maxima from the first and second derivatives of the bed elevation from model output.

Following Overeem et al. (2022), the a-priori effect of ice was quantified with the non-dimensional ice-dominance ratio I,

$$I = \frac{Q_{\text{ice}}}{Q_{\text{river}}}$$

In this ratio, $Q_{\text{ice}} = \int_{t=t_{\text{ice}}} Q_s(t)\,dt$ (in kg), which represents the integrated fluvial sediment flux ($Q_s(t)$, kg/s) delivered when nearshore sea-ice is present (t_{ice}). The term $Q_{\text{river}} = \int_{t\neq t_{\text{ice}}} Q_s(t)\,dt$ is remainder of the fluvial sediment load, which is delivered when there is no nearshore sea ice. For temperate deltas, $I = 0$, and for fully ice-dominated deltas $I = \infty$. Note that this ratio includes t_{ice} for winter ice-cover, although that was not simulated in the model seasonal run since the Colville sediment discharge nearly ceases during this period (Table 2; Figure 3a).

4. Results

Model outputs are separated into four subsections: Section 4.1 compares the morphodynamics between ice-affected and ice-free delta developmental cases and highlights the unique ice-driven features on centennial timescales; Section 4.2 presents results on seasonal differences in the ice-affected simulation; Section 4.3 compares long-term delta simulations with and without waves; and Section 4.4 shows the changes in clinoform morphology produced by warming Arctic climate conditions on decadal timescales.

4.1. Effects of Ice on Delta Development (Ice-Free, Ice-Affected, and Ice-Matrix Simulations)

The presence of nearshore sea ice had a notable impact on deltaic clinoform development and morphology. In contrast to the clinoform that developed during ice-free simulations, the ice-affected delta developed a compound clinoform but differed in subaerial and subaqueous morphology (Figure 4).

For long-term delta development simulations (1500 years), the ice-free delta formed a single, "Gilbert-type" clinoform with a subaerial topset extending 9 km offshore, whereas the ice-affected delta formed a compound clinoform with a 7.8 km subaerial and a 1.8 km subaqueous topset (Figure 4). Early in delta development (100 years), progradation distances and aggradation rates between the two runs were equal (Figures 4e and 4f). However, as clinoform growth transitioned to be dominantly progradational, the ice-affected delta encountered the 2-m thick sea ice floating 1 km offshore. Changes in water depths from sea ice constrained the flow and generated shear stresses exceeding the critical shear stress for erosion (0.80 N/m^2) during the break-up season in the topset region. Ice-induced shear stresses remained elevated for an additional 2 km offshore compared to the ice-free scenario. These elevated shear stresses promoted sediment bypassing in the nearshore zone that resulted in the development of a subaqueous delta.

Due to bypassing, ice-affected deltas experienced slower subaerial delta progradation rates compared with ice-free scenarios (Figures 4e and 4f). On the ice-affected delta, the shoreline did not extend until 700 years into the simulation, almost halfway through the total model runtime. Until the 700-year timestamp, on average, 95% of

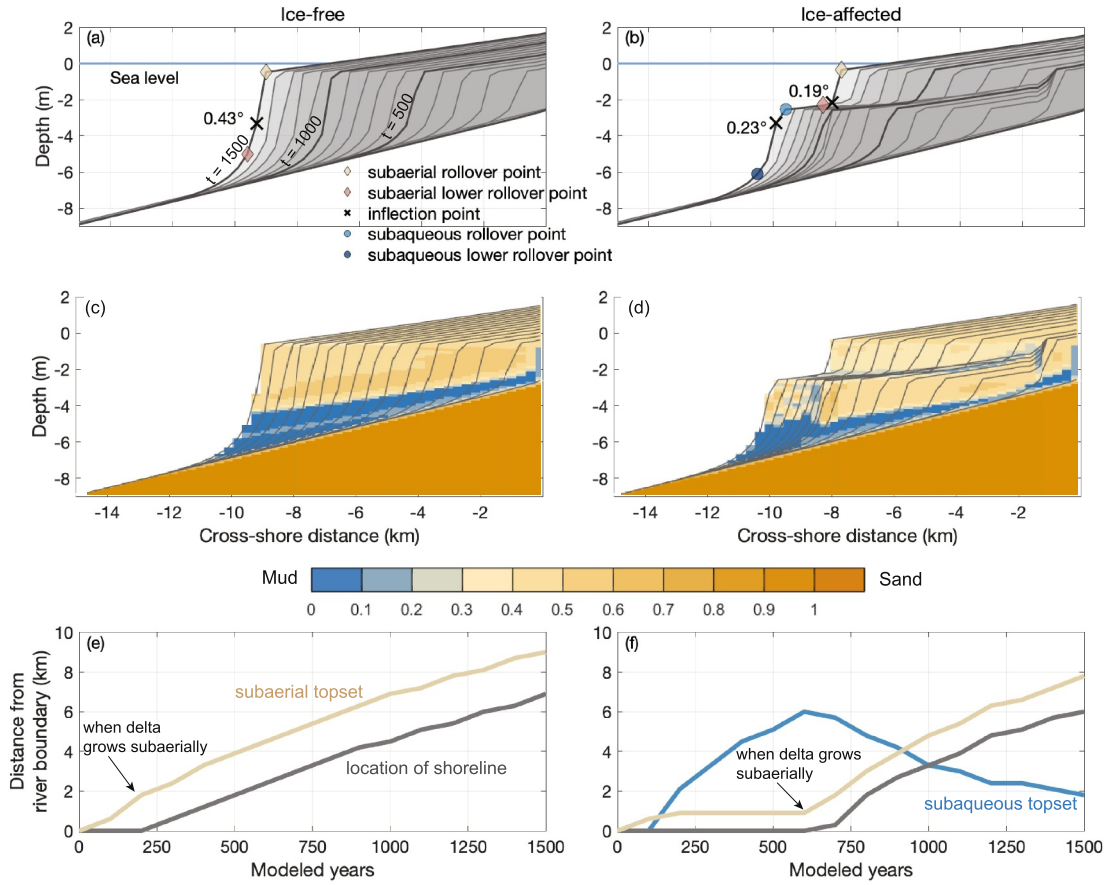

Figure 4. Long-term delta developmental results for: (a) ice-free and (b) ice-affected. Dark gray lines highlight morphology after 500, 1,000, and 1,500 years of delta growth, as denoted in plot (a). See figure key for the location of rollover and inflection points. Foreset gradients are in degrees and displayed to the left of the inflection point. The internal sediment composition of ice-free and ice-affected results are shown in (c) and (d). Length of the subaerial (tan) and subaqueous (blue) topsets, and shoreline position (gray) relative to modeled time for (e) ice-free and (f) ice-affected simulations.

the annual sediment load went to develop the 6 km long subaqueous delta. Floating sea ice then moved a grid cell (300 m) seaward with shoreline progradation by our model design. This adjustment in ice location during break-up promoted deposition to the subaerial portion of the delta and influenced the ice-affected delta progradation, where on average 71% and 29% of the annual sediment load went to the subaerial and subaqueous deltas, respectively, after the shoreline developed.

Both the ice-free and ice-affected simulations produced a coarsening-upward stratigraphy, with mud accumulating on the foreset and prodelta and sand accumulating on the topset (Figures 4c and 4d). Mixing of deltaic mud and sand basement occurred at the delta base and prodelta. But, in the ice-influenced delta, sand accumulated on both the subaerial and subaqueous topsets and created a mud "pocket" in the subaerial foreset that ranged from 68% to 87% mud content (Figure 4d). The sedimentary sequencing showed sand depositing in low-relief regions of the subaqueous platform, indicating a transition to the subaqueous topset in the stratigraphic record (Figure 4d). At the final timestamp for the ice-affected simulation (1500 years), the top 60 cm of the subaerial topset comprised ~43% sand, whereas the subaqueous topset was ~31% sand (Figure 4d).

The compound clinoform morphology produced by ice was highly dependent on ice location, depth, and corresponding river hydrodynamics (Figure 5). Cases from "ice-matrix" simulations where ice was closer to the river mouth developed a compound clinoform earlier in delta development (Figures 5a–5c), and cases that featured thicker ice developed subaqueous deltas farther from shore in deeper water (Figures 5c and 5f). Relative lengths of the subaqueous topset increased with ice thickness (Figure 5j). Additionally, lengths were overall greater when sea ice was closer to shore. When sea ice was located farther offshore (2 km), a compound clinoform did not develop (Figures 5g–5j). In this case, there was not enough flow confinement to promote sediment bypassing.

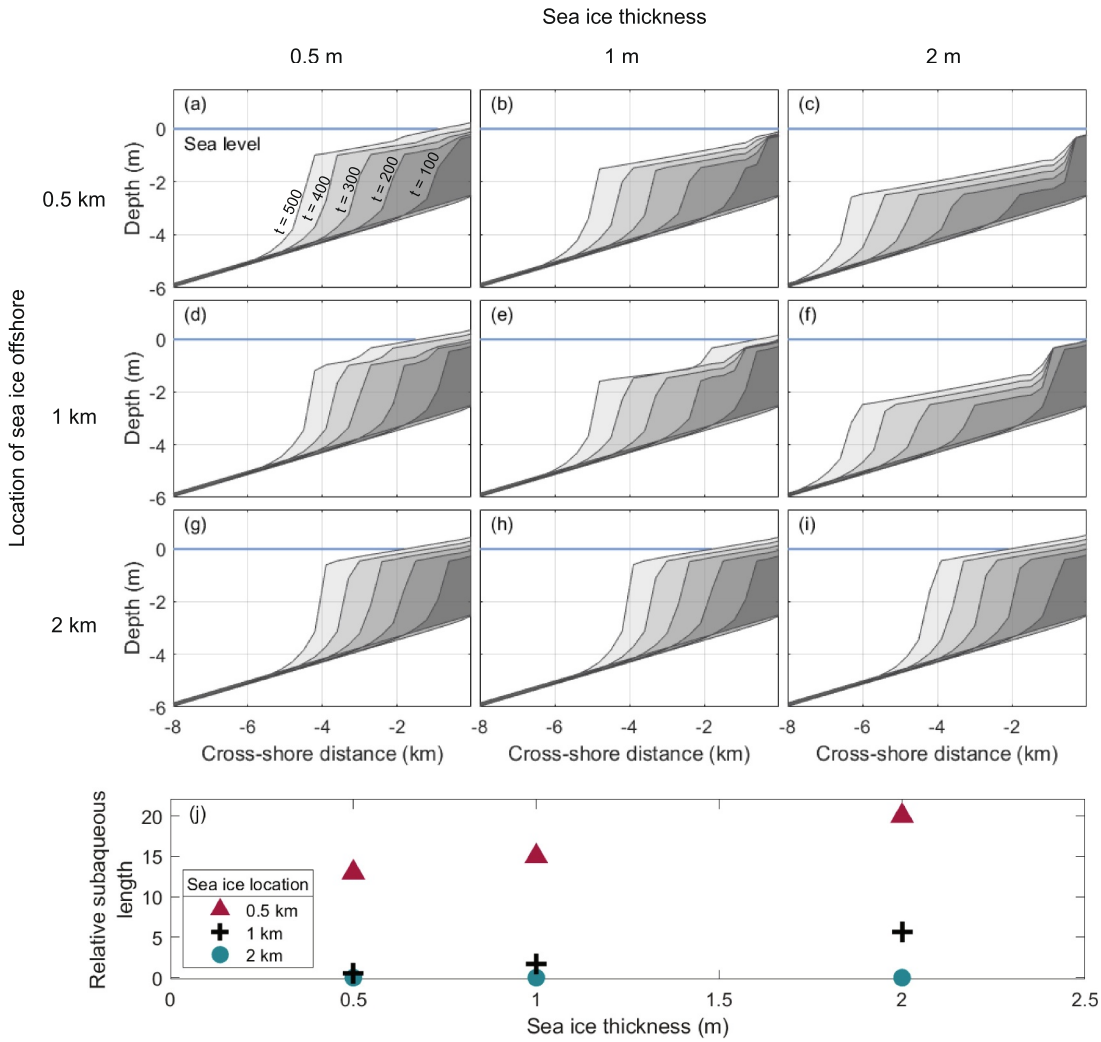

Figure 5. Ice matrix simulations testing various locations and depths of sea ice in the model (a–i). Dark-to-light gray denotes the timestamps at 100–500 years as shown in plot a. (j) Relative length of the subaqueous topset compared to the subaerial topset by the assigned sea ice thickness and location.

4.2. Impacts of Seasonality on Ice-Affected Delta Development

The seasonal variations in hydro- and morphodynamics can explain the long-term delta development. In an annual simulation, the seasonal contribution to total delta volume was as follows: break-up, 28%; open-water, 69%; and freeze-up, 3%. These contributions corresponded to the sediment discharge assigned at the river boundary and duration of the given season (Table 2). However, within each season, sediment dispersal spatially varied and therefore shaped different regions of the modeled delta (Figures 6a–6f).

The break-up season depositional patterns were strongly dependent on the distance between the river mouth and the floating sea ice. On average, 147% of the sediment discharge during break-up was deposited in the subaqueous delta, meaning erosional processes were active on the subaerial portion of the delta (Figures 6a and 6d). The greatest cross-shore currents and bed shear stresses occurred during the break-up season. High discharge under sea ice promoted currents up to 95 cm/s and peak shear stresses of 1.5 N/m^2. These conditions occurred at the subaerial foreset to subaqueous topset transition where sea ice was located. At times, the combination of strong flows and elevated water levels led to the erosion of subaerial deposits by amounts almost equivalent in volume to subaerial deposits formed during the open-water season (Figures 6d and 6e).

During the open-water season, 86% and 14% of the fluvial sediment load was deposited on the subaerial and the subaqueous deltas, respectively. This depositional pattern was constant throughout the 1500-year simulation and

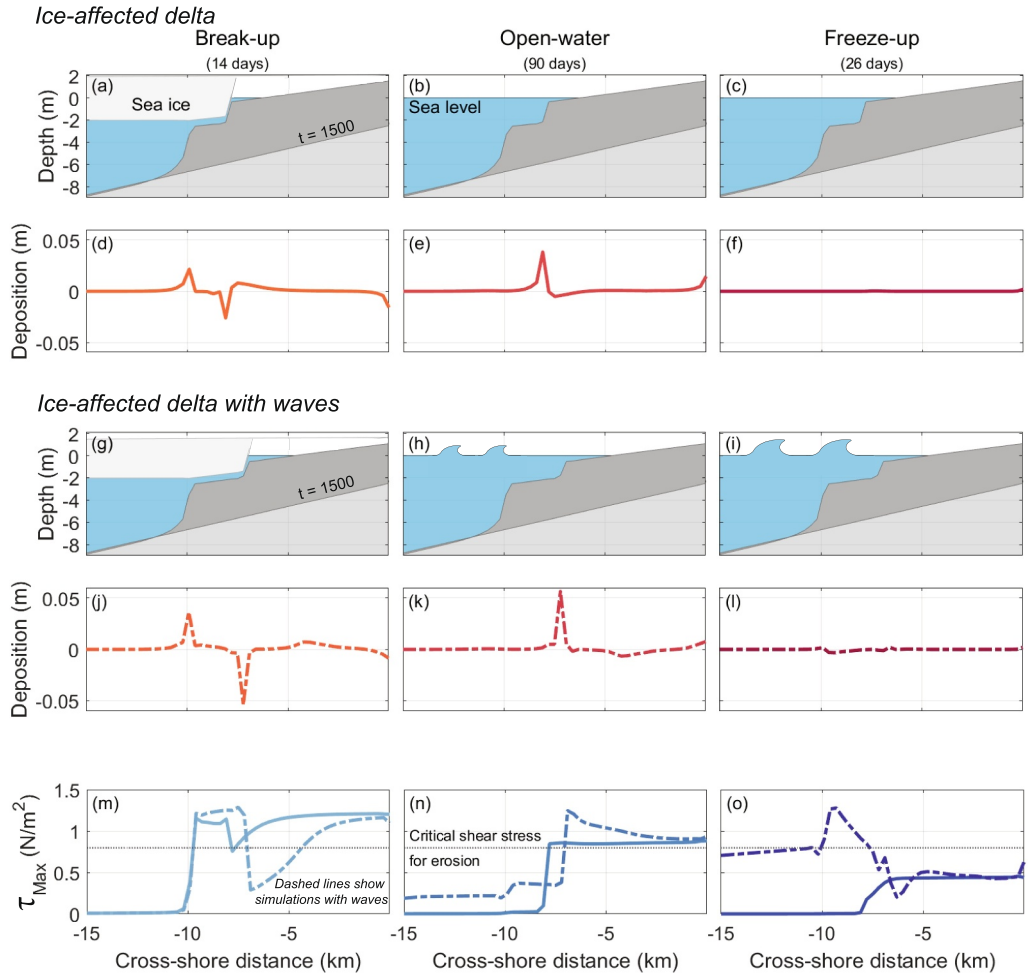

Figure 6. Seasonal morpho- and hydrodynamics at the 1500-year timestamp on the ice-affected delta and ice-affected delta with waves. (a–c) Bathymetry and water level for ice-affected delta for each season. (d–f) Total seasonal deposition as a function of cross-shore distance, highlighting location of depocenters. (g–i) Bathymetry and water level for ice-affected delta with waves for each season. (j–l) Location of deposition in the simulation with waves. (m–o) Maximum critical shear stresses for erosion during the individual seasons and simulations.

was ultimately responsible for the development and seaward progradation of the subaerial delta. Maximum sustained river currents during the open-water season were 73 cm/s on the shallow subaerial topset. Sediment accumulation occurred at the subaerial foreset at rates up to 7.1 cm/yr.

During freeze-up, 100% of the incoming fluvial sediments were deposited on the subaerial topset. Flow velocities were typically lowest during freeze-up because this period received the lowest seasonal discharge (Table 2). However, this trend changed with the inclusion of waves, which is further discussed in the following section.

The ice-dominance ratio I for the ice-affected delta is 5.4, that is, 84% of the annual sediment delivery occurred when there was nearshore sea ice, and the remaining 16% of the annual sediment load occurred when no sea ice was present. The modeled ratio is below the average I-ratio observed on the Colville Delta, which is 67.2 (Figure 3), and is most comparable to the measured conditions in 2012 and 2016, which had I ratios of 6.0 and 5.0, respectively (Figure 3a).

4.3. Wave Influence on Ice-Free and Ice-Affected Delta Development

A moderate wave climate was added to the open-water and freeze-up seasons in the ice-free and ice-affected scenarios (Table 2; Figure 7), interacting with the delta for ~50 days out of the 130-day annual cycle. Wave inputs reflected the lowest 5% of wave heights in the ERA5 record offshore the Colville during sequential seasons

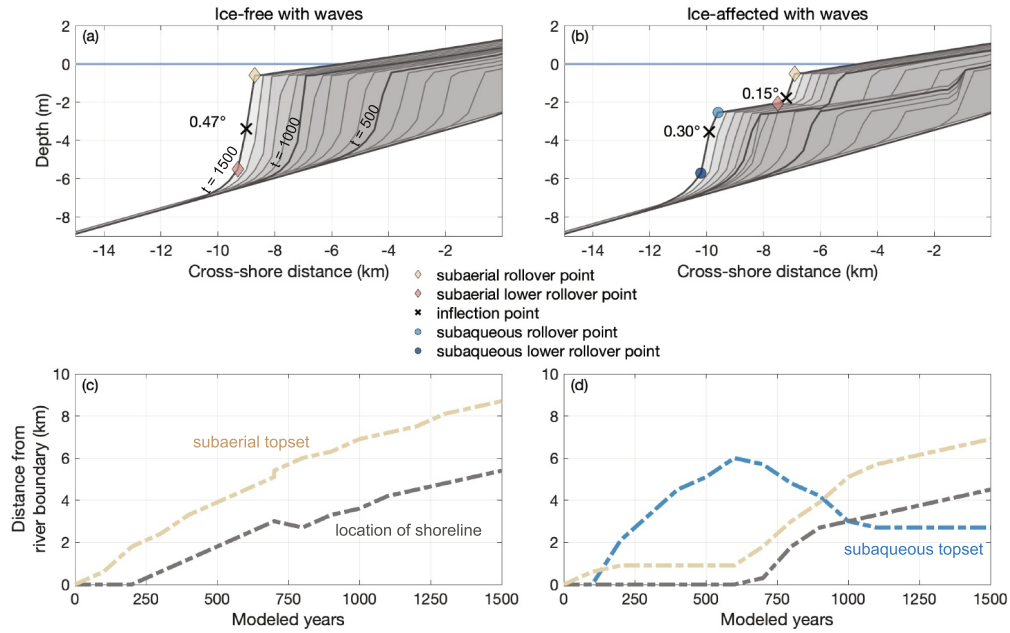

Figure 7. Long-term delta development with waves results for: (a) ice-free and (b) ice-affected. Dark gray lines highlight timestamps after 500, 1,000, and 1,500 years of delta growth as denoted in plot (a). See figure key for the location of rollover and inflection points. Foreset gradients are in degrees and displayed to the left of the inflection point. Length of the subaerial (tan) and subaqueous (blue) topsets, and shoreline position (gray) relative to modeled time for (c) ice-free and (d) ice-affected simulations.

(Figure S1 in Supporting Information S1). Waves began when the subaerial delta aggraded to 0.8 m above mean sea level, to prevent overtopping and influencing the river boundary, and lasted for the remainder of the 1500-year simulation.

On the ice-affected delta, the introduction of waves increased maximum shear-stresses from 1.1 to 1.3 N/m^2 and from 0.5 to 1.3 N/m^2 in the open-water and freeze-up seasons, respectively (Figures 6n and 6o). Open-water and freeze-up wave climates affected different portions of the delta. Smaller waves shoaled closer inshore during the open-water season, which deepened the subaerial rollover point by 0.16 m and decreased delta aggradation rates overall (Figure 7). However, the larger wave climate imposed during freeze-up affected the subaqueous portion of the delta, with waves shoaling at depths near the subaqueous rollover point. Over time, this increased wave climate steepened the gradient of the subaqueous foreset from 0.23° to 0.30° (Figure 7). Notably, waves diminished shoreline progradation rates, which created a morphologic feedback in the model with the location of ice. As mentioned in Section 3.2.1, the floating sea ice moves seaward with shoreline growth; therefore, in the simulation featuring sea ice and waves, sea ice remained closer to the delta apex compared to the simulation without waves. The combined processes of sea ice nearshore and wave-driven sediment dispersal aided in the growth of the subaqueous delta, lengthening the subaqueous topset from 1.8 to 2.1 km compared to long-term simulation without waves (Figure 7).

In the ice-free simulation, the inclusion of waves had a smaller impact on delta morphology than in the ice-affected. The imposed wave climate steepened the gradient of the delta shoreface from 0.43° to 0.47° (Figures 4a and 7a) and increased the separation between the shoreline and subaerial rollover point (Figure 7c). It should be noted that because waves started in the simulation based on delta elevation, the ice-free scenario experienced waves for 200 years more than the ice-affected scenario.

4.4. Future Morphologic Change in Arctic Deltas

Two future sea-state scenarios were run to represent Arctic delta morphologic response to a prolonged open-water period and an intensified wave climate (partially resulting from the prolonged open-water period) The ice-dominance ratio for these future scenarios is 4.6, which is lower than any of the ratios measured on the Colville Delta from the 2003–2016 record and 16% lower than the long-term simulations (Figure 3a). Simulations ran

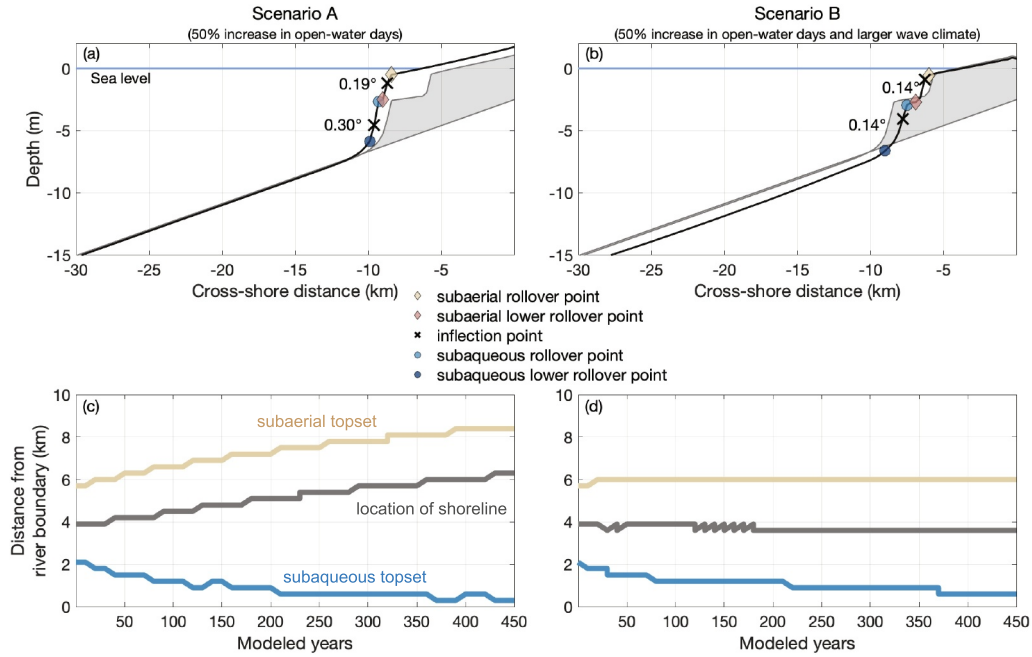

Figure 8. Deltas produced from future scenarios after 450 years: (a) clinoform morphology after a 50% increase in open-water days and (b) clinoform morphology after a 50% increase in open-water days *and* a larger wave climate with 0.8 and 2 m wave heights with a 7 s period. Lighter gray clinoform is the starting bathymetry used at the beginning of the simulation. The black line shows the final result of the simulation. The position of the shoreline (gray) and lengths of subaerial (tan), and subaqueous (blue) topsets relative to modeled time are shown in (c) scenario A and (d) scenario B.

for a total of 450 years using the starting bathymetry from the 1100-year timestamp of the long-term evolution model with sea ice and waves. Future scenario model inputs are described in Table 2.

4.4.1. Scenario A: 50% More Open-Water Days

The expansion of the open-water season resulted in rapid sediment infill of the shallow subaqueous delta (Figure 8a). After 250 years, the subaqueous topset was reduced from 2.0 km to 0.3 km in width (Figure 8c). However, the subaqueous delta was not entirely removed to produce a single clinoform at the end of the simulation. Since sea ice remained present during break-up, sediment bypassing still occurred, as noted in the long-term model runs, and promoted outbuilding of the subaqueous delta. Moreover, bypassing was highly dependent on the location of the sea ice relative to the shoreline.

In scenario A, break-up produced the highest shear stresses of 1.30 N/m^2 due to substantial discharge. Notably, the increase in the time of wave action had little effect on overall delta morphology during the open-water season. Shear stresses were similar to those exhibited in the long-term ice-affected case with waves because both simulations featured the same prescribed wave climate (Table 2). The rollover points deepened by 0.039 and 0.098 m on the subaerial and subaqueous deltas (Figure 8a). At approximately the 350-year mark, the rate of morphologic change decelerated for the lengths of the subaerial and subaqueous topsets, indicating that extending the model run time to 500 years would likely result in minimal to no change to the overall delta morphology (Figure 8c).

4.4.2. Scenario B: Intensified Wave Climate

Increases in wave heights and period during the open-water and freeze-up seasons resulted in a different delta morphology compared to scenario A, though still maintaining a compound clinoform morphology (Figure 8). At the beginning of the simulation, waves attenuated from 2 to 1 m at the wave base offshore the delta and again between the subaqueous and subaerial rollovers by 0.4 m before shoaling at the shoreline. Over time, the wave energy eroded the subaqueous topset width from 2.0 to 0.6 km and hindered subaerial delta progradation (Figures 8b and 8d). Wave action created a concave-upward inner shelf that progressively deepened and moved

landward during the simulation. This concave-upward profile resembles the inner shelf currently present on the Colville (Figures 1c and 8b).

Maximum shear stresses doubled during the freeze-up season compared to scenario A, increasing from 1.3 to 2.9 N/m^2. Deposition during break-up appeared to have a minor overall effect on delta morphology, with most of the deposition eroded by waves during the following seasons. Throughout the 450-year simulation, the subaqueous rollover point deepened by 0.26 m while the subaerial rollover point decreased by 0.48 m in depth (Figure 8b). Notably, the subaerial topset exhibited little to no rate of morphologic change in scenario B compared to scenario A, whereas comparable rates were observed for the change in length of the subaqueous topset between the two simulations (Figures 8c and 8d).

5. Discussion

Based on the Delft3D simulations, we found that the subaqueous 2-m platform observed offshore of Arctic deltas —which resembles a subaqueous delta topset observed in lower-latitude deltaic clinoforms—can be generated from river forcing and floating landfast sea ice alone (i.e., without waves, which are thought to help create this geometry in non-polar settings). We explore how sea ice alters delta morphology and how longer open-water seasons and larger waves may re-shape Arctic deltas and affect the dispersal of Arctic riverine sediments to offshore depocenters.

5.1. Sea Ice Effects on Cross-Shelf Delta Morphodynamics

As detailed in Section 4.1, the ice-affected delta displays the defining characteristics of a compound clinoform. The delta profile comprises a coupled subaerial and subaqueous delta with corresponding rollover points, separated by a low-relief region of minimal accumulation (Patruno & Helland-Hansen, 2018; Peng et al., 2020; Pirmez et al., 1998; Swenson et al., 2005). Both subaerial and subaqueous portions of the clinoform have a basinward dipping topset-foreset-bottomset morphology, which progrades seaward through time (Figures 1a and 4b). Similarly, the ice-affected delta exhibits a more sigmoidal geometry associated with compound clinoforms compared to the oblique single clinoform formed during the ice-free simulation and more typical of lower-latitude systems (Patruno et al., 2015; Swenson et al., 2005; Figure 4). Furthermore, the modeled ice-affected delta has the same internal stratigraphic architecture associated with a compound clinoform—namely, seaward-dipping beds as well as coarser sediments comprising the subaerial and subaqueous topsets and finer sediments comprising the foresets (Lim et al., 2019; Peng et al., 2020; Figure 4).

Morphodynamics in the ice-affected simulations exemplify the impacts of nearshore sea ice on sediment dispersal. Ice reduces nearshore deposition and promotes sediment bypassing, resulting in enhanced seaward progradation of the shallow subaqueous platform (Figures 4 and 7). Our findings are in agreement with the reduced complexity models (RCM) developed by Chan et al. (2023), Piliouras et al. (2021), and Lauzon et al. (2019), which simulated the generation of a subaqueous 2-m platform in the presence of ice (in planform view). For example, in the most recently developed RCM by Chan et al. (2023), a ∼1–3 km 2-m ramp developed around the delta apex after 150 years from the presence of 2-m thick ice, matching the 2-m depth and 1.2 km extension we simulated at the same timescale and thickness (Figure 4f).

In non-polar environments, this type of sediment bypassing is usually driven by waves and/or tidal currents in deltas where waves are <2 m and tidal ranges are >2 m (J. P. Walsh & Nittrouer, 2009; Figure 1a). In these wave- or tide-influenced settings, high near-bed shear stresses from wave orbital velocities and tidal currents create a lateral separation between the river mouth and the region of high sediment accumulation (i.e., a subaqueous foreset, or compound morphology; Peng et al., 2020; Swenson et al., 2005; J. P. Walsh & Nittrouer, 2009; Figure 1a). Similar processes of compound clinoform development were observed in modeled ice-affected deltas, but in the absence of large tidal ranges or intense wave energy. This finding has implications for stratigraphic interpretations of ancient deltas, which may exhibit a morphology previously interpreted as a high-energy wave and/or tide-dominated system, but alternatively, it may result from the presence of nearshore sea ice in a low-energy environment.

The compound clinoforms strongly depend on the sea ice thickness and location. In the ice matrix simulations, when spring-time ice was located far from the river mouth (2 km, mimicking an earlier summertime decay of sea ice), sediments deposited near shore before contacting the sea ice and thus formed a single clinoform (Figures 5g–

5i). In contrast, the presence of thicker ice closer to shore promoted a greater sustained current under ice, resulting in a larger lateral separation between the subaerial and subaqueous clinoforms (Figures 5a–5f and 5j). These contrasting results suggest that a critical nearshore sea ice thickness (compared to the fluvial channel depth) and distance from shore (compared to the potential progradation during spring) are required to form a compound clinoform from ice processes. These non-dimensional comparisons suggest that there is an effect of sea-ice on delta clinoforms if it lies closer than 37% of the spring progradation distance offshore, and is thicker than 20% of the channel depth. This provides a ratio of required accommodation space (i.e., less space nearshore due to ice = extended subaqueous delta) needed for subaqueous topset development. These findings are similar to those reported by Chan et al. (2023), who examined the timing of ice melt and basin slope, and further suggests that a critical nearshore sea ice condition is needed in addition to seasonal sediment flux during ice-presence (Q_{ice}) to form a compound clinoform from ice processes.

5.2. Impacts of Arctic Seasonality

The inclusion of seasonality (i.e., timing and extent of ice relative to high river discharge) resulted in different depositional patterns on ice-affected deltas. During the breakup season, sea ice promoted seaward advection of sediments, and a depocenter formed offshore (Figure 6). In contrast, a more proximal depocenter formed during the summertime open-water season on the subaerial foreset (Figures 6d and 6e) because of reduced sediment discharge as well as increased nearshore accommodation space in the absence of ice. Also, despite sediment loads from the river being higher during breakup, the most morphologic development occurred during the summertime open-water season (a result which is consistent with the RCM by Chan et al., 2023 which measured a 4 times increase total delta area with the inclusion of summertime discharge). This result may have important implications for Arctic fluvial carbon delivery, insomuch as carbon may be stored in different locations on the delta (and at different water depths) during different seasons (McClelland et al., 2016; Raymond et al., 2007).

Despite the greater degree of morphologic change in summer, however, the springtime dispersal pattern modulated by sea ice must act as a long-term control on Arctic delta morphology since only Arctic deltas exhibit the shallow 2-m subaqueous platform and undergo the process of ice break-up (Are & Reimnitz, 2000; Reimnitz & Bruder, 1972). Previous studies have found that compound clinoform morphology can be driven by event-based influences (e.g., floods, storms), which vary in duration, frequency, and magnitude (Fagherazzi & Overeem, 2007; Swenson et al., 2005). Therefore, the annual event of break-up likely impacts delta morphology in the same way as episodic storms. In other words, two depocenters develop on the modeled ice-affected delta: (a) on the distal foreset, promoted by sediment bypassing under sea ice during spring flood conditions (analogous to storm-driven transport in lower-latitude systems) and (b) on the proximal foreset during the open-water season when "normal"/low-energy (fair-weather) conditions occur on the delta, and seaward progradation of the subaerial part of the delta occurs (see Swenson et al., 2005 for a non-polar model). Despite differences in the length of the open-water season (90 days) compared to the break-up season (14 days), at times, these depocenters were similar in volume of deposition—but the impacts on morphology are very different. To summarize, Arctic delta shoreline progradation is more likely to occur in the open-water season, while the compound morphology is primarily developed during the break-up season. This finding has important implications considering the lengthening open-water seasons in the Arctic (Barnhart et al., 2016; Bliss et al., 2019; see Section 5.5).

5.3. Wave Impacts

The shallow geometry of Arctic continental shelves is known to limit the coastal morphodynamic impacts from waves (Malito et al., 2022; Overeem et al., 2022). We observed wave heights decrease 50% at ~27 m isobath and another 60% at the 2-m ramp, confirming the subaqueous platform's ability to decrease wave energy acting on the shoreline (Overeem et al., 2022). In long-term simulations, wave energy at the 2–3 m isobath decreased on average 39% and 84% during open-water and freeze-up seasons, respectively. These seasonal waves increased seabed slopes on the delta topset and foresets, limited shoreline progradation, and aided subaqueous delta development (Figure 7).

However, waves likely created a feedback with the location of ice and shoreline in the model since ice moved seaward with shoreline development. The decline in shoreline progradation rates from wave reworking kept sea ice closer to shore for the following break-up season and slowed overall delta progradation, thus moving the delta closer to a steady state, as illustrated in Figure 7d. This modeled relationship between waves and the location of

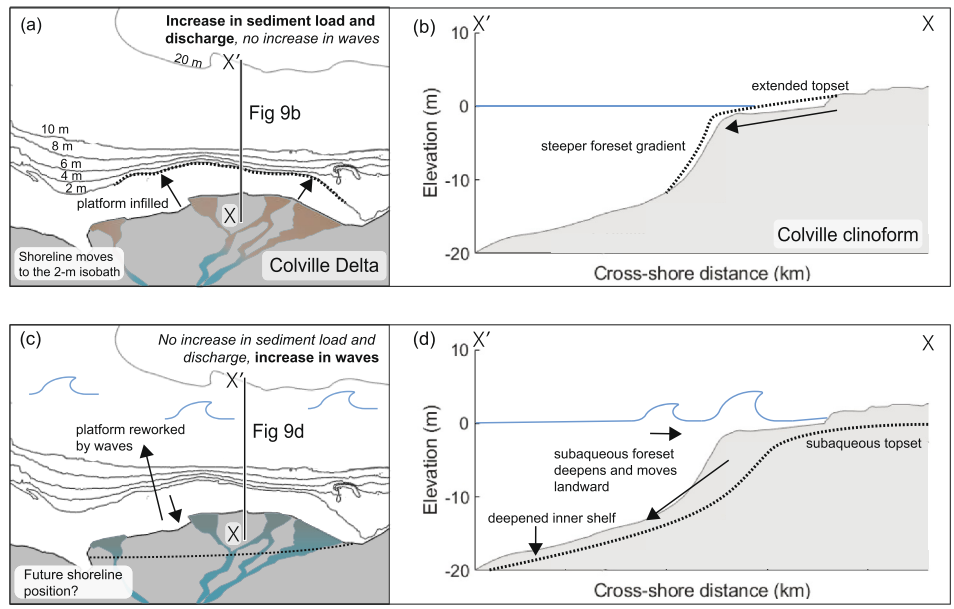

Figure 9. Conceptual diagram of Colville River Delta morphology based on the future scenario simulations. (a) Plan-view of the Colville Delta based on dominating future river conditions; (b) Cross-sectional view of the Colville clinoform based on dominating future river conditions; (c) Plan-view of the Colville Delta based on dominating future wave conditions; (d) Cross-sectional view of the Colville clinoform based on dominating future wave conditions.

nearshore sea ice could indicate another factor limiting Arctic delta progradation rates and maintaining the 2-m subaqueous feature (Overeem et al., 2022). Storm waves and surges continue into the ice-free season, removing deltaic sediments from these sediment-starved systems (Reimnitz, 2002). Therefore, storm-induced erosion could balance sea ice-driven transport by controlling shoreline location, thus helping maintain the current delta structure.

5.4. Future Arctic Delta Morphology

As the Arctic loses ice due to warming temperatures, ice influence on Arctic deltas will decrease and river and wave influences will increase (Overeem et al., 2022). We simulated changes in ice and river influence by increasing the length of the open-water season, and simulated changes in wave influence by imposing larger waves (see Section 4.4; Figure 3c and Figure S1 in Supporting Information S1).

In scenario A, the length of the open-water season was increased by 50%, and the delta transitioned from a compound clinoform to a simpler, Gilbert-style delta over a period of 450 years (Figures 8, 9a, and 9b). The reduction in sea ice duration meant that the nearshore accommodation space increased. This change, coupled with increased fluvial supply due to a longer open-water season, led to rapid sediment infilling near shore and subaerial delta progradation (Figure 8). In other words, the delta became more river-dominated and less ice-dominated.

The simulated effect of scenario A is consistent with Chan et al. (2023), who used the climate-model projections of future sediment discharge and ice conditions (Stocker, 2013) to model the future morphology of the Lena Delta and saw the 2-m subaqueous feature infill after 200 years. The results presented here also raise questions about the future of the Colville Delta in the coming centuries. In the model, the 50% increase in annual open-water days (from 90 to 135 days) resulted in an increase in wave exposure from 50 to 70 days and an increase in overall season of fluvial sediment delivery from 130 to 175 days per year. By comparison, the Colville Delta has experienced waves for an average of 106 days per year in the last 20 years (Figure S1 in Supporting Information S1). Will the delta begin prograding if the number of open-water and fluvial delivery days increases?

It is worth noting that the progradation modeled in scenario A depends on the available fluvial sediment fluxes. Notably, the sediment supply in our future scenarios did not increase in concentration, but rather only in the duration of delivery. However, climate models predict increases in Arctic river sediment fluxes from warming temperatures as a result of permafrost thaw (Syvitski, 2002; Zhang et al., 2022). Such an increase in fluvial

sediment flux would make the infilling modeled in scenario A more likely in the coming decades. This prediction is illustrated in our conceptual diagram for scenario A (Figures 9a and 9b).

In contrast to scenario A, scenario B was dominated by erosional processes (Figures 8, 9c, and 9d). The inputs and open-water season timing were the same as in scenario A, but wave heights and periods were larger (Table 2). Simulated conditions mimic those recently observed offshore of the Colville Delta later in the open-water and freeze-up seasons (Figure 3c). At the end of 450 years, the 2-m subaqueous topset was reduced from 2.1 to 0.9 km in width. Despite effective wave attenuation across the subaqueous topset, the annual recurrence of larger waves ultimately led to excessive erosion and created a morphologic feedback whereby increasingly large waves propagated to the shoreline (resulting in a 45% increase in wave energy at the shore) and the subaqueous platform deepened. Thus, if the regional wave climate further increases as predicted (Casas-Prat & Wang, 2020b), the subaqueous delta may entirely erode, and the subaerial delta may erode as well if marine sediment erosion exceeds fluvial supply. These dynamics could ultimately transition the current compound morphology to a marine-dominated dispersal system with features resembling those of wave-dominated deltas along high-energy shelves (J. P. Walsh & Nittrouer, 2009). This prediction for scenario B is shown in Figures 9c and 9d. The transition from ice-driven to wave-driven transport would significantly change the delta morphologic processes of the Colville Delta and other Arctic deltas exposed to a similar growing wave climate and alter fundamental land-ocean interactions from excess erosion.

Notably, both scenarios are modeled separately here but are likely to occur simultaneously: A longer open-water season will expand the fetch that drives the increase in wave energy. As a result, the contrasting transitions of both scenarios will compete with uncertain outcomes in terms of river- or wave-dominance. Change may occur soon though. An increase of 50% in open water days can drive substantial changes in delta morphology. This finding implies that Arctic deltas do not need to experience 365-day open-water periods to transition from ice-affected deltas to river- or wave-dominated features. A recent projection suggests that the Arctic winters may be ice-free by 2100 (Barnhart et al., 2016). If true, the model results presented here suggest that Arctic deltas may experience substantial morphologic change much earlier than that. Furthermore, inputs in the model are based on current field observations; thus, Arctic deltas may already be transitioning from ice-dominated systems to river- and/or wave-dominated systems.

5.5. Recommendations

The 1D model developed in this study is helpful for interpretations and predictions of Arctic delta formation under the influence of sea ice, as well as future evolution under reduced sea ice, different seasonality (in the river and/or ocean), or absence of sea ice. Our results from these analyses highlight several areas for further investigation.

First, the implementation of a floating structure in Delft3D effectively mimicked the effects of landfast ice and can be used to explore ice dynamics in future Delft3D polar simulations. However, the structure does not allow for any wave propagation or water flow over the floating structures. Nederhoff et al. (2022) recently adapted SWAN to incorporate wave dissipation by ice, which could be implemented in the model as an alternative to the floating structure during seasonal transitions. Including these more sophisticated wave interactions with sea ice would further enhance our understanding of wave-damping and wave stresses in the nearshore region and on the subaqueous delta. This could also assist in better addressing the potential sediment flux contributed by waves, Q_{wave}, on the deltaic environment (Overeem et al., 2022).

Second, cryosphere processes in addition to sea ice, such as permafrost thaw, play an essential role in the morphologic framework of Arctic deltas (Overeem et al., 2022; Piliouras & Rowland, 2020). Frozen permafrost sediments armor the coastline and seabed from erosive processes during break-up and freeze-up, which stabilizes deltaic sediments and leads to even distribution of fluvial sediments at the delta shoreline (see models by: Chan et al., 2023; Lauzon et al., 2019; Piliouras et al., 2021). In the present study, erodibility never varied with the seasons, and exploring the effects of a thawing coastline on delta evolution would be a valuable future investigation.

Lastly, the modeled delta developed a 2-m subaqueous topset or "ramp" under sea ice from riverine forcing, which possessed the architecture of a subaqueous clinoform typical of a compound delta. However, these 2-m submerged platforms are also observed—though with narrower widths (e.g., 0.5–5 km)—on Arctic coastlines which receive little fluvial sediment during spring break-up. Reimnitz (2002) suggest two alternative explanations

for how ice-driven processes could produce this shallow feature: (a) repetitive erosion by tidal currents during the ice-covered season induced by tidal cracks between landfast ice and seabed; and (b) storm-induced coastal setup in the fall with the presence of landfast ice that moves sediment seaward due to horizontal pressure gradients. Thus, a more comprehensive future model would benefit from the inclusion of these more complex hydrodynamics to better understand ice-mediated delta evolution and the nuances of subaqueous topset formation in polar versus lower-latitude environments.

6. Conclusions

This study simulated Arctic delta development and compared it to deltas with no ice, such as those in lower-latitude regions. Our analysis of 12 modeled clinoforms shows that sea ice-driven processes altered fluvial sediment deposition and promoted sediment bypassing offshore, generating a compound clinoform. However, morphologic characteristics heavily depend on offshore conditions (e.g., location of nearshore ice, seasonality, shallow inner shelf). We found that nearshore sea ice characteristics controlled the morphology of the subaqueous delta, with thicker ice closer to shore resulting in a larger lateral separation between the subaerial and subaqueous clinoforms (i.e., a wider subaqueous topset).

Additionally, our study highlighted the various depositional patterns which occur during different Arctic seasons and mediate how the delta morphology evolves. We found that during the open-water season, sediment was routed to a different depocenter compared with the break-up period. The open-water sea depocenter supplied the subaerial delta and contributed more to overall delta growth. Furthermore, the Arctic fall storm climate may assist in maintaining the subaqueous topset by limiting shoreline progradation.

Most notably, our future modeled simulations suggest that the Colville Delta may already be shifting in its morphologic influence from ice- to river- or wave-dominated due to reduced seasonal sea ice coverage. Both future scenarios resulted in a strong reduction of the 2-m subaqueous topset in the 450-year simulation. With the extended ice-free conditions, fluvial sediments infilled the shallow nearshore region. However, extended ice-free conditions with an intensified Arctic wave climate gradually eroded the subaqueous topset. The loss of this crucial feature, which serves as a buffer for shoreline erosion by waves, will alter morphologic processes on Arctic deltas and could make them more vulnerable to wave action at the shorelines during the open-water and freeze-up seasons. Furthermore, changes in Arctic delta morphology would affect the future delivery of fluvial sediment, nutrients, and carbon sequestration in Arctic coastal systems.

Data Availability Statement

Model simulations were conducted using Delft3D-FLOW coupled with modules written in MATLAB and outputs were processed in MATLAB. Model output files and examples can be found at the Arctic Data Center (Cooper et al., 2023). Delft3D is an open-access modeling package available for download at Deltares (https://download.deltares.nl/delft3d-4-suite). Inputs for model simulations were downloaded from open-access data portals. Bathymetric data offshore the Colville can be found through IBCAO (Jakobsson et al., 2020) and Zimmermann et al. (2022). The seabed inputs used in the model can also be found at the Arctic Data Center (Eidam, 2023). River gauge data were accessed from the USGS data portal for the Colville River (U.S. Geological Survey, 2022). Historic river sediment data were extracted from Arnborg et al. (1967) figures using the Juicr Package in R Studio (Lajeunesse, 2021). European Center for Medium-Range Weather Forecast ERA5 wave reanalysis together with sea ice ARC MFC reanalysis were downloaded from the Copernicus Service catalogue (Arctic Ocean Wave Hindcast, 2022).

Acknowledgments
This research was funded by the US National Science Foundation (OPP 1913195). We would like to thank our collaborators Nina Stark and Nick Brilli for their assistance in data collection and analysis, the *R/V Utpika* team for their field support, and Li Erikson (USGS) for providing gridded NOS nearshore data of Harrison Bay. Additionally, thank you to the three anonymous reviewers who provided helpful expert insights to improve this manuscript.

References

Arctic Ocean Wave Hindcast. (2022). E.U. Copernicus marine service information [Dataset]. *Marine Data Store*. https://doi.org/10.48670/moi-00008

Are, F., & Reimnitz, E. (2000). An overview of the Lena River Delta setting: Geology, tectonics, geomorphology, and hydrology. *Journal of Coastal Research*, *16*(4), 1083–1093.

Arnborg, L., Walker, H. J., & Peippo, J. (1966). Water discharge in the Colville River, 1962. *Geografiska Annaler - Series A: Physical Geography*, *48*(4), 195–210. https://doi.org/10.1080/04353676.1966.11879739

Arnborg, L., Walker, H. J., & Peippo, J. (1967). Suspended load in the Colville River, Alaska, 1962. *Geografiska Annaler - Series A: Physical Geography*, *49*(2/4), 131–144. https://doi.org/10.2307/520882

Barnhart, K. R., Miller, C. R., Overeem, I., & Kay, J. E. (2016). Mapping the future expansion of Arctic open water. *Nature Climate Change*, *6*(3), 280–285. https://doi.org/10.1038/nclimate2848

Barnhart, K. R., Overeem, I., & Anderson, R. S. (2014). The effect of changing sea ice on the physical vulnerability of Arctic coasts. *The Cryosphere*, *8*(5), 1777–1799. https://doi.org/10.5194/tc-8-1777-2014

Bliss, A. C., Steele, M., Peng, G., Meier, W. N., & Dickinson, S. (2019). Regional variability of Arctic sea ice seasonal change climate indicators from a passive microwave climate data record. *Environmental Research Letters*, *14*(4), 045003. https://doi.org/10.1088/1748-9326/aafb84

Boggs, S. J. (1995). In R. A. McConnin (Ed.), *Principles of sedimentology and stratigraphy* (2nd ed.). Prentice-Hall, Inc.

Box, J. E., Colgan, W. T., Christensen, T. R., Schmidt, N. M., Lund, M., Parmentier, F. J. W., et al. (2019). Key indicators of Arctic climate change: 1971–2017. *Environmental Research Letters*, *14*(4), 045010. https://doi.org/10.1088/1748-9326/aafc1b

Brilli, N. (2023). *Influence of geotechnical properties on sediment dynamics, erodibility, and geomorphodynamics in coastal environments based on field measurements* (Doctoral dissertation). Virginia Tech. Retrieved from VTechWorks

Casas-Prat, M., & Wang, X. L. (2020a). Projections of extreme ocean waves in the Arctic and potential implications for coastal inundation and erosion. *Journal of Geophysical Research: Oceans*, *125*(8), e2019JC015745. https://doi.org/10.1029/2019JC015745

Casas-Prat, M., & Wang, X. L. (2020b). Sea ice retreat contributes to projected increases in extreme Arctic Ocean surface waves. *Geophysical Research Letters*, *47*(15), e2020GL088100. https://doi.org/10.1029/2020GL088100

Chan, N. H., Langer, M., Juhls, B., Rettelbach, T., Overduin, P., Huppert, K., & Braun, J. (2023). An Arctic delta reduced-complexity model and its reproduction of key geomorphological structures. *Earth Surface Dynamics*, *11*(2), 259–285. https://doi.org/10.5194/esurf-11-259-2023

Cooper, C., Eidam, E., & Nienhuis, J. (2023). 1500, 500, and 450-year Sea Ice models and output morphology data, Colville River Delta, Alaska [Dataset]. *Arctic Data Center*. https://doi.org/10.18739/A2XG9FC7G

Dammann, D. O., Eriksson, L. E. B., Mahoney, A. R., Stevens, C. W., Sanden, J. V. D., Eicken, H., et al. (2018). Mapping Arctic bottomfast sea ice using SAR interferometry. *Remote Sensing*, *10*(5), 1–17. https://doi.org/10.3390/rs10050720

de Goede, E., Wagner, T., de Graaff, R., & Sheets, B. (2014). Modelling of ice growth and transport on a regional scale, with application to Fountain Lake, Minnesota, USA. In *Paper presented at OMAE2014* (pp. 1–8).

Deltares. (2014). *Delft3D flow user manual version 4.05.79018*. Deltares. Retrieved from www.deltares.nl/en/software-and-data

Eidam, E. F. (2023). Seabed grain-size data from Harrison Bay (Beaufort Sea continental shelf), Alaska 2021 [Dataset]. *Arctic Data Center*. https://doi.org/10.18739/A2JW86P50

Eidam, E. F., Brilli, N., Cooper, C., Duncan, D., Nienhuis, J. H., & Stark, N. (2022). Morphology and sediments of the subaqueous Colville River Delta (Alaska). In *Poster presented at 2022 AGU Fall Meeting*.

Eidam, E. F., Cooper, C., Heath, A., Nienhuis, J., & Seim, H. (2023). Summertime sediment-transport dynamics on an Arctic continental shelf. In *Poster presented at 2023 AGU Fall Meeting*.

Eidam, E. F., Nittrouer, C. A., Ogston, A. S., DeMaster, D. J., Liu, J. P., Nguyen, T. T., & Nguyen, T. N. (2017). Dynamic controls on shallow clinoform geometry: Mekong Delta, Vietnam. *Continental Shelf Research*, *147*, 165–181. https://doi.org/10.1016/j.csr.2017.06.001

Fagherazzi, S., & Overeem, I. (2007). Models of deltaic and inner continental shelf landform evolution. *Annual Review of Earth and Planetary Sciences*, *35*(1), 685–715. https://doi.org/10.1146/annurev.earth.35.031306.140128

Galloway, W. E. (1975). Process framework for describing the morphologic and stratigraphic evolution of deltaic systems. In *Deltas, Models for Exploration* (pp. 87–98).

Gibbs, A. E., & Richmond, B. M. (2015). *National assessment of shoreline change—Historical shoreline change along the North Coast of Alaska, U.S.-Canadian Border to Icy Cape* (p. 96). U.S. Geological Survey Open File Report 2015–1048. https://doi.org/10.3133/ofr20151048

Gilbert, G. K. (1885). *The topographic features of lake shores*. United States Geological Survey, 5th Annual Report (p. 123).

Hošeková, L., Malila, M. P., Rogers, W. E., Roach, L. A., Eidam, E. F., Rainville, L., et al. (2020). Attenuation of ocean surface waves in Pancake and Frazil Sea Ice along the coast of the Chukchi Sea. *Journal of Geophysical Research: Oceans*, *125*(12), e2020JC016746. https://doi.org/10.1029/2020JC016746

Jakobsson, M., Mayer, L. A., Bringensparr, C., Castro, C. F., Mohammad, R., Johnson, P., et al. (2020). The international bathymetric chart of the Arctic Ocean version 4.0 [Dataset]. *Scientific Data*, *7*(1), 176. https://doi.org/10.1038/s41597-020-0520-9

Kasper, J. L., & Weingartner, T. J. (2014). The spreading of a buoyant plume beneath a landfast ice cover. *American Meteorological Society*, *45*(2), 478–494. https://doi.org/10.1175/JPO-D-14-0101.1

Lajeunesse, M. J. (2021). Automated, semi-automated, and manual extraction of numerical data from scientific images, plot, charts, and figures. (Version 0.1) [Software]. *R package*. Retrieved from https://cran.r-project.org/package=juicr

Lauzon, R., Piliouras, A., & Rowland, J. C. (2019). Ice and permafrost effects on delta morphology and channel dynamics. *Geophysical Research Letters*, *46*(12), 6574–6582. https://doi.org/10.1029/2019GL082792

Lesser, G. R., Roelvink, J. A., van Kester, J. A. T. M., & Stelling, G. S. (2004). Development and validation of a three-dimensional morphological model. *Coastal Engineering*, *51*(8–9), 883–915. https://doi.org/10.1016/j.coastaleng.2004.07.014

Lim, Y., Levy, J. S., Goudge, T. A., & Kim, W. (2019). Ice cover as a control on the morphodynamics and stratigraphy of Arctic deltas. *Geology*, *47*(5), 399–402. https://doi.org/10.1130/G45146.1

Mahoney, A., Eicken, H., Gaylord, A. G., & Shapiro, L. (2007). Alaska landfast sea ice: Links with bathymetry and atmospheric circulation. *Journal of Geophysical Research*, *112*, 1–18. https://doi.org/10.1029/2006JC003559

Malito, J., Eidam, E. F., & Nienhuis, J. (2022). Increasing wave energy moves arctic continental shelves toward a new future. *Journal of Geophysical Research: Oceans*, *127*(9), e2021JC018374. https://doi.org/10.1029/2021JC018374

McClelland, J. W., Holmes, R. M., Peterson, B. J., Raymond, P. A., Striegl, R. G., Zhulidov, A. V., et al. (2016). Particulate organic carbon and nitrogen export from major Arctic rivers. *Global Biogeochemical Cycles*, *30*(5), 629–643. https://doi.org/10.1002/2015GB005351

Meier, W. N., & Stroeve, J. (2022). An updated assessment of the changing Arctic sea ice cover. *Oceanography*, *35*(3/4), 10–19. https://doi.org/10.12952/journal.elementa.000010

Mikhailova, M. V. (2009). Hydrological processes at an Arctic river mouth: Case study of the Colville River, Alaska, USA. *Water Resources*, *36*(1), 26–42. https://doi.org/10.1134/S0097807809010035

Nederhoff, K., Erikson, L., Engelstad, A., Bieniek, P., & Kasper, J. (2022). The effect of changing sea ice on wave climate trends along Alaska's central Beaufort Sea coast. *The Cryosphere*, *16*(5), 1609–1629. https://doi.org/10.5194/tc-16-1609-2022

Nienhuis, J. H., Ashton, A. D., Edmonds, D. A., Hoitink, A. J. F., Kettner, A. J., Rowland, J. C., & Törnqvist, T. E. (2020). Global-scale human impact on delta morphology has led to net land area gain. *Nature*, *577*(7791), 514–518. https://doi.org/10.1038/s41586-019-1905-9

Orton, G. J., & Reading, H. G. (1993). Variability of deltaic processes in terms of sediment supply, with particular emphasis on grain size. *Sedimentology*, *40*(3), 475–512. https://doi.org/10.1111/j.1365-3091.1993.tb01347.x

Overeem, I., Nienhuis, J. H., & Piliouras, A. (2022). Ice-dominated Arctic deltas. *Nature Reviews Earth & Environment*, *3*(4), 225–240. https://doi.org/10.1038/s43017-022-00268-x

Patruno, S., Hampson, G. J., & Jackson, C. A. L. (2015). Quantitative characterisation of deltaic and subaqueous clinoforms. *Earth-Science Reviews*, *142*, 79–119. https://doi.org/10.1016/j.earscirev.2015.01.004

Patruno, S., & Helland-Hansen, W. (2018). Clinoforms and clinoform systems: Review and dynamic classification scheme for shorelines, subaqueous deltas, shelf edges and continental margins. *Earth-Science Reviews*, *185*(3), 202–233. https://doi.org/10.1016/j.earscirev.2018.05.016

Pellegrini, C., Patruno, S., Helland-Hansen, W., Steel, R. J., & Trincardi, F. (2020). Clinoforms and clinothems: Fundamental elements of basin infill. *Basin Research*, *32*(4), 187–205. https://doi.org/10.1111/bre.12446

Peng, Y., Olariu, C., Steel, R. J., Peng, Y., & Olariu, C. (2020). Recognizing tide- and wave-dominated compound deltaic clinothems in the rock record. *Geology*, *48*(12), 1149–1153. https://doi.org/10.1130/G47767.1

Piliouras, A., Lauzon, R., & Rowland, J. C. (2021). Unraveling the combined effects of ice and permafrost on Arctic delta morphodynamics. *Journal of Geophysical Research: Earth Surface*, *126*(4), 1–17. https://doi.org/10.1029/2020JF005706

Piliouras, A., & Rowland, J. C. (2020). Arctic River delta morphologic variability and implications for riverine fluxes to the coast. *Journal of Geophysical Research: Earth Surface*, *125*(1), 1–20. https://doi.org/10.1029/2019JF005250

Pirmez, C., Pratson, L. F., & Steckler, S. (1998). Clinoform development by advection-diffusion of suspended sediment: Modeling and comparison to natural systems. *Journal of Geophysical Research*, *103*(B10), 24141–24157. https://doi.org/10.1029/98JB01516

Pratson, L. F., Nittrouer, C. A., Wiberg, P. L., Steckler, M. S., Swenson, J. B., Cacchione, D. A., et al. (2007). Seascape evolution on clastic continental shelves and slopes. *Continental Margin Sedimentation*, 339–380. https://doi.org/10.1002/9781444304398.ch7

Rawlins, M. A., Cai, L., Stuefer, S. L., & Nicolsky, D. (2019). Changing characteristics of runoff and freshwater export from watersheds draining northern Alaska. *The Cryosphere*, *13*(12), 3337–3352. https://doi.org/10.5194/tc-13-3337-2019

Raymond, P. A., McClelland, J. W., Holmes, R. M., Zhulidov, A. V., Mull, K., Peterson, B. J., et al. (2007). Flux and age of dissolved organic carbon exported to the Arctic Ocean: A carbon isotopic study of the five largest Arctic rivers. *Global Biogeochemical Cycles*, *21*(4), 2007GB002934. https://doi.org/10.1029/2007GB002934

Reimnitz, E. (2002). Interactions of river discharge with sea ice in proximity of Arctic deltas: A review. *Polarforschung*, *70*(1–2), 123–134.

Reimnitz, E., & Bruder, K. (1972). River discharge into an ice-covered ocean and related sediment dispersal, Beaufort Sea, Coast of Alaska. *The Geological Society of America Bulletin*, *83*(3), 861–866. https://doi.org/10.1130/0016-7606(1972)83[861:rdiaio]2.0.co;2

Reimnitz, E., Graves, S. M., & Barnes, P. W. (1985). *Beaufort Sea coastal erosion, shoreline evolution, and sediment flux* (Vol. 85–380, pp. 78). U.S. Geological Survey Report.

Reimnitz, E., Toimil, L., & Barnes, P. (1978). Arctic continental shelf morphology related to sea-ice zonation, Beaufort Sea, Alaska. *Marine Geology*, *28*(3–4), 179–210. https://doi.org/10.1016/0025-3227(78)90018-X

Smith, M., & Thomson, J. (2016). Scaling observations of surface waves in the Beaufort Sea. *Elementa*, *2016*(1), 1–12. https://doi.org/10.12952/journal.elementa.000097

Stocker, T. (2013). In *Climate Change 2013: The Physical Science Basis: Working Group I Contribution to the Fifth Assessment Report of the Intergovernmental Panel on Climate Change*. Cambridge University Press.

Stroeve, J., & Notz, D. (2018). Changing state of Arctic sea ice across all seasons. *Environmental Research Letters*, *13*(10), 103001. https://doi.org/10.1088/1748-9326/aade56

Swenson, J. B., Paola, C., Pratson, L., Voller, V. R., & Murray, A. B. (2005). Fluvial and marine controls on combined subaerial and subaqueous delta progradation: Morphodynamic modeling of compound-clinoform development. *Journal of Geophysical Research*, *110*(F2), 1–16. https://doi.org/10.1029/2004JF000265

Syvitski, J. (2002). Sediment discharge variability in Arctic rivers: Implications for a warmer future. *Polar Research*, *21*(2), 323–330. https://doi.org/10.3402/polar.v21i2.6494

Syvitski, J., Cohen, S., Miara, A., & Best, J. (2019). River temperature and the thermal-dynamic transport of sediment. *Global and Planetary Change*, *178*, 168–183. https://doi.org/10.1016/j.gloplacha.2019.04.011

Thomson, J., Fan, Y., Stammerjohn, S., Stopa, J., Rogers, W. E., Girard-Ardhuin, F., et al. (2016). Emerging trends in the sea state of the Beaufort and Chukchi seas. *Ocean Modelling*, *105*, 1–12. https://doi.org/10.1016/j.ocemod.2016.02.009

Thomson, J., & Rogers, W. E. (2014). Swell and sea in the emerging Arctic Ocean. *Geophysical Research Letters*, *41*(9), 3136–3140. https://doi.org/10.1002/2014GL059983

U.S. Geological Survey. (2022). National water information system data available on the World Wide Web (USGS Water Data for the Nation). https://doi.org/10.5066/F7P55KJN

Walker, H. J. (1973). Spring discharge of an Arctic River determined from salinity measurements beneath sea ice. *Water Resources Research*, *9*(2), 474–480. https://doi.org/10.1029/WR009i002p00474

Walker, H. J. (1994). Environmental impact of river Dredging in Arctic Alaska (1981–89). *Arctic*, *47*(2), 176–183. https://doi.org/10.14430/arctic1287

Walker, H. J. (1998). Arctic deltas. *Journal of Coastal Research*, *14*(3), 718–738.

Walker, H. J., & Hudson, P. F. (2003). Hydrologic and geomorphic processes in the Colville River delta, Alaska. *Geomorphology*, *56*(3–4), 291–303. https://doi.org/10.1016/S0169-555X(03)00157-0

Walsh, J. E., Eicken, H., Redilla, K., & Johnson, M. (2022). Sea ice breakup and freeze-up indicators for users of the Arctic coastal environment. *The Cryosphere*, *16*(11), 4617–4635. https://doi.org/10.5194/tc-16-4617-2022

Walsh, J. P., & Nittrouer, C. A. (2009). Understanding fine-grained river-sediment dispersal on continental margins. *Marine Geology*, *263*(1–4), 34–45. https://doi.org/10.1016/j.margeo.2009.03.016

Weingartner, T. J., Danielson, S. L., Potter, R. A., Trefry, J. H., Mahoney, A., Savoie, M., et al. (2017). Circulation and water properties in the landfast ice zone of the Alaskan Beaufort Sea. *Continental Shelf Research*, *148*, 185–198. https://doi.org/10.1016/j.csr.2017.09.001

Zhang, T., Li, D., East, A. E., Walling, D. E., Lane, S., Overeem, I., et al. (2022). Warming-driven erosion and sediment transport in cold regions. *Nature Reviews Earth & Environment*, *3*(12), 832–851. https://doi.org/10.1038/s43017-022-00362-0

Zimmermann, M., Erikson, L. H., Gibbs, A. E., Prescott, M. M., Escarzaga, S. M., Tweedie, C. E., et al. (2022). Nearshore bathymetric changes along the Alaska Beaufort Sea coast and possible physical drivers. *Continental Shelf Research*, *242*, 104745. https://doi.org/10.1016/j.csr.2022.104745